The Potential Effect of Nav1.8 in Autism Spectrum Disorder: Evidence from A Congenital Case with Compound Heterozygous SCN10A Mutations

Björn Heinrichs
RWTH Aachen University Medical Faculty
Baowen Liu
Tongji Hospital of Tongji Medical College of Huazhong University of Science and Technology
Jin Zhang
Tongji Hospital of Tongji Medical College of Huazhong University of Science and Technology
Jannis Meents
RWTH Aachen University
Kim Le
RWTH Aachen University Medical Faculty: Rheinisch-Westfalische Technische Hochschule Aachen Medizinische Fakultat
Petra Hautvast
RWTH Aachen University Medical Faculty: Rheinisch-Westfalische Technische Hochschule Aachen Medizinische Fakultat
Xiwen Zhu
Chongqing Medical University
Ningbo Li
Tongji Hospital of Tongji Medical College of Huazhong University of Science and Technology
Yi Liu
Tongji Hospital of Tongji Medical College of Huazhong University of Science and Technology
Markus Rothermel
RWTH Aachen University Medical Faculty
Barbara Namer
RWTH Aachen University Medical Faculty: Rheinisch-Westfalische Technische Hochschule Aachen Medizinische Fakultat
Xianwei Zhang
Tongji Hospital of Tongji Medical College of Huazhong University of Science and Technology
Angelika Lampert
RWTH Aachen University Medical Faculty
Guangyou Duan (dgy1986anesthesia@126.com)

Chongqing University of Medical Science Clinical College: The Second Affiliated Hospital of Chongqing Medical University https://orcid.org/0000-0002-6199-7882

Research

Keywords: SCN10A/Nav1.8, autism spectrum disorder (ASD), genetic, mutation

Posted Date: October 6th, 2020

DOI: https://doi.org/10.21203/rs.3.rs-77513/v1

Title page

Research paper

The potential effect of $Na_v1.8$ in autism spectrum disorder: Evidence from a congenital case with compound heterozygous *SCN10A* mutations

Björn Heinrichs[1,*], Baowen Liu[2,3,*], Jin Zhang[3], Jannis E. Meents[1], Kim Le[4], Petra Hautvast[1], Xiwen Zhu[2], Ningbo Li[3], Yi Liu[1,3], Markus Rothermel[4], Barbara Namer[5], Xianwei Zhang[3], Angelika Lampert[1,#], Guangyou Duan[2,#].

[1]Institute of Physiology, Medical Faculty, RWTH Aachen University, 52074 Aachen, Germany.

[2]Department of Anesthesiology, The Second Affiliated Hospital, Chongqing Medical University, Chongqing, 400010, China.

[3]Department of Anesthesiology, Tongji Hospital, Tongji Medical College, Huazhong University of Science and Technology, Wuhan 430030, China.

[4]Department of Chemosensation, AG Neuromodulation, Institute for Biology II, RWTH Aachen University, Aachen 52074, Germany.

[5] Research group neurosciences of the Interdisciplinary Center for Clinical Research (IZKF) within the faculty of Medicine at the RWTH Aachen University, 52074 Aachen, Germany

*These authors contributed equally to this work.

Correspondence: Guangyou Duan (dgy1986anesthesia@126.com) or Angelika Lampert (alampert@ukaachen.de).

Running title: The role of $Na_v1.8$ in autism spectrum disorder

Abstract

Background

Apart from the most prominent symptoms in Autism spectrum disorder (ASD), namely deficits in social interaction and repetitive behavior, patients often show abnormal sensory reactivity to environmental stimuli. Especially potentially painful stimuli are reported to be experienced in a different way compared to healthy persons.

Methods

In our present study, we present an ASD patient carrying compound heterozygous mutations in the voltage-gated sodium channel (VGSC) $Na_v1.8$, which is preferentially expressed in sensory neurons. We expressed both identified mutations, p.I1511M and p.R512X, in a heterologous expression system and investigated their biophysical properties using patch-clamp recordings.

Results

The results of these experiments suggest that both mutations lead to different degrees of loss-of-function of $Na_v1.8$. Behavioral experiments in a $Na_v1.8$ loss-of-function mouse model additionally revealed $Na_v1.8$ may play a role in autistic behavior.

Limitations

Our study did not verified the functions of p.I1511M and p.R512X mutations in vivo. The mice with these mutations can be constructed to verify the mutation functions in the future investigations. In addition, since we have only found one ASD patient which may relate to SCN10A mutations, the role of Nav1.8 in ASD needs to be confirmed in more cases. Moreover, the cellular mechanism underlying the effect of Nav1.8 on ASD needed to be explored in future studies.

Conclusions

Our results present $Na_v1.8$ as a protein potentially involved in ASD pathophysiology and may therefore offer new insights to the genetic basis of this disease.

Keywords: *SCN10A*/$Na_v1.8$; autism spectrum disorder (ASD); genetic;

mutation

Introduction

Autism or autism spectrum disorder (ASD) is a complex neurodevelopmental disorder with multiple symptoms affecting cognitive, social, communication and emotional processes that emerge during infancy and persist throughout life. Recently, it was reported that the prevalence of ASD is about 1.46-2.50%, which has steadily increased over the past decades[1-3]. The study of ASD has made great strides in the recent years, but the pathophysiological mechanism of ASD remains unclear. It is widely accepted that the causes of ASD include environmental and genetic factors[4]. Genetic factors are thought to contribute more substantially than environmental factors and the influence of genetic factors in autism etiology is estimated to be about 50-90%[4-7]. Moreover, there are hundreds of genes associated with ASD, suggesting that autism has a strong, but complex genetic component. Therefore, investigating ASD patients with genetic variants may offer new ways in understanding the pathophysiology of the disease.

Numerous studies have revealed changes in expression or function of genes involved in neurodevelopment as the main genetic cause of ASD[8]. Excitation/inhibition imbalance is a very popular hypothesis in the pathogenesis of autism[9]. It is known that voltage-gated sodium channels (VGSCs) play important roles in excitability of neurons and the mutations of VGSC genes result in a wide range of peripheral and central nervous system disorders[10-12].

Here, we identified a child diagnosed with ASD, and investigated potentially causative genes using a screening sequencing chip for neuropsychiatric disorders. The results revealed two destructive, compound-heterozygous variants in *SCN10A*, which were found to be inherited from mother and father, respectively. *SCN10A*/$Na_v1.8$ belongs to the family of VGSCs and has been considered as a critical factor in the initiation of action potentials in nervous systems[13], and there is evidence for a role of *SCN10A*/$Na_v1.8$ in the development of pain disorders[14-16]. Interestingly, it has been demonstrated by questionnaire and neuroimaging studies that nociception of ASD patients is commonly disturbed[17-19].

A small part of ASD cases have been reported to be monogenic in origin[20]. Therefore, the mutations of *SCN10A* in our patient may be the best candidate etiology for the ASD phenotype in this case. However, there is no published case of ASD caused by *SCN10A* mutations so far.

In this study, we aimed to explore the potential role of *SCN10A*/$Na_v1.8$ in the development of ASD. Mutation analysis and whole-cell voltage-clamp were used to investigate the effect of the mutations of *SCN10A* on the biophysical properties of $Na_v1.8$. $Na_v1.8$ knockout mice were used as an animal model to explore whether loss of $Na_v1.8$ results in ASD-like behaviors.

Methods

Clinical investigations

The study regarding this rare case of ASD was approved by the hospital ethics committee of The Second Affiliated Hospital of Chongqing Medical University, and informed consent was obtained from all subjects.

Genetic screening and mutation analysis

The patient received a genetic testing using a screening chip including 6110 different target genes related to neurological function by SINOPATH DIAGNOSIS company (Beijing, China) when he was three years old. Two heterozygous mutations in *SCN10A* were identified. Because *SCN10A* mutations have not been described to play a role in ASD, we performed a whole genome sequencing for the patient through high-throughput sequencing when he was four years old. During the process of the treatment at the age of five, the patient received a whole exome sequencing. At that time, we also collected blood samples and performed *SCN10A* sanger sequencing (primer sequences are shown in *Supplementary Table 1*) for the patient and his family members. Mutation analysis and function prediction was performed through SIFT, Ployphen-2 and Mutation Taster[21-23].

Mutagenesis

We generated the $hNa_v1.8$/R512X and $hNa_v1.8$/I1511M mutant plasmids in a pIRESpuro3 vector by site-directed mutagenesis using Q5 polymerase (New England Biolabs, Ipswich, MA, USA).

Cell culture and transfection

For electrophysiological examination of the mutations, we used the neuroblastoma cell line ND7/23 (hybrid of mouse neuroblastoma and rat dorsal root ganglion cells). The cells were cultured in Dulbecco's modified Eagle's medium (DMEM, Gibco Life Technologies, Carlsbad, CA, USA), supplemented with 4.5 g/L glucose, 10% fetal bovine serum (Gibco Life Technologies, Carlsbad, CA, USA) and 1% penicillin/streptomycin (Sigma Aldrich, St. Louis, MO, USA).

To achieve optimal conditions for transfection, cells were seeded 24-48 hours before transfection. Transfection was performed using jetPEI transfection reagent (Polyplus transfection, Illkirch, France). For each transfection a total amount of 1.5 µg DNA was used, consisting of 1.25 µg $hNa_v1.8$ plasmid (WT, I1511M or R512X) and 0.25 µg GFP. Patch-clamp recordings were performed 24-36 hours after transfection.

Electrophysiology

Transfected ND7/23 cells were recorded using an EPC 10 USB patch-clamp amplifier (HEKA Electronics, Lambrecht, Germany). The sampling rate was 50 kHz with a 10 kHz low-pass Bessel filter. Patch pipettes were pulled using a DMZ pipette puller (Zeitz-Instrumente Vertriebs GmbH, Martinsried, Germany). Pipettes with a tip resistance in the range of 0.9 to 2.2 MΩ were used. Only green fluorescent cells were chosen for patch-clamp recordings. Experiments were performed at room temperature (22 ± 1 °C). The liquid junction potential of 8.7 mV was corrected for prior to the recordings.

The extracellular solution (ECS) contained the following: 140 mM NaCl, 1 mM $MgCl_2$, 1 mM $CaCl_2$, 10 mM HEPES, 10 mM TEA-Cl and 10 mM glucose. The osmolarity of the ECS was 303 mOsm/L and the pH was adjusted to 7.3 with NaOH.

Endogenous sodium currents of ND7/23 cells were inhibited by 500 nM tetrodotoxin (TTX, Tocris Bioscience, Bristol, UK) added to the bath solution. The intracellular solution (ICS) consisted of 2 mM NaCl, 140 mM CsF, 1 mM EGTA, 10 mM HEPES and 10 mM TEA-Cl. The osmolarity of the ICS was 295-296 mOsm/L and the pH was adjusted to 7.2 with CsOH.

Series resistance compensation was 70-80% and only cells with a series resistance of less than 5.5 MΩ throughout the recordings were included in the analysis. The P/4 procedure was used for online leak current subtraction. After establishing the whole-cell configuration, cells were held at -120 mV and stimulated to 0 mV with a frequency of 0.1 Hz for 5 min to stabilize sodium currents.

Voltage protocols

Voltage dependence of activation was investigated by 40 ms depolarizing pulses between -80 and +70 mV in 10 mV steps every 5 seconds. For each cell, we determined the reversal potential for sodium (V_{rev}) and calculated the conductance (G) at each voltage step (V) with the equation $G = \frac{I}{V - V_{rev}}$, with I being the measured sodium current at the respective voltage step. The conductance-voltage relationship was fitted with a Boltzmann function: $\frac{G}{G_{max}} = G_{min} + \frac{G_{max} - G_{min}}{1 + e^{\frac{V_{half} - V_m}{k}}}$, with G_{min} and G_{max} being the minimum and maximum sodium conductance, V_{half} the potential of half maximal activation, V_m the membrane potential and k the slope factor. In our analysis, G_{min} was set to 0 and G_{max} to 1.

Current density was calculated for each cell by dividing the maximum sodium current that occurred during the recordings for the voltage dependence of activation by the cell's capacitance. The mean current remaining at 30 to 35 ms after onset of the voltage pulse was measured as the persistent current. Persistent current density was calculated equally to current density.

For each voltage pulse with enough inward current, we also measured the delay from voltage pulse onset to the time point of maximal sodium current (time to peak, TTP). The relationship between TTP and voltage was fitted with an exponential decay function: $t = (t_0 - t_{plateau}) * e^{-\frac{V_m}{\tau}} + t_{plateau}$ (t = TTP at the respective voltage, t_0

= TTP at the lowest analyzed voltage step [in our case -10 mV], $t_{plateau}$ = offset from zero of the decay function, V_m = membrane potential, τ = decay constant)

The decay of inward sodium current after reaching its peak could be fitted with a two-phase exponential decay function: $I = I_{span,fast} * e^{-\frac{t}{\tau_{fast}}} + I_{span,slow} * e^{-\frac{t}{\tau_{slow}}} + I_{plateau}$ (I = sodium current at a certain time after current peak, $I_{span,fast}$ = current range of the fast decay component, $I_{span,slow}$ = current range of the slow decay component, $I_{plateau}$ = offset from zero of the decay function, t = time after peak of the sodium current, τ_{fast} = decay constant of the fast decay component, τ_{slow} = decay constant of the slow decay component). This fit was done again for every voltage pulse with enough inward current (in our case starting at -10 mV). The development of the decay constants over the different potentials was afterwards plotted and compared.

The voltage dependence of fast inactivation was investigated with a protocol consisting of two pulses. Firstly, a 500 ms pre-pulse to potentials varying between -150 and 0 mV in 10 mV steps was used to drive channels into fast inactivated states. Afterwards, the channels remaining in the resting state were activated by a 40 ms test pulse to +40 mV. These two pulses were repeated every 10 seconds. The measured current (I) was normalized to the maximum current in any of the voltage pulses (I_{max}) and plotted against the voltage of the pre-pulse (V). The current voltage-relationship was fitted with a Boltzmann function as described above with G_{max} set to 1.

Steady-state slow inactivation was investigated similar to fast inactivation, but with a three-pulse protocol. At first, a 10 ms pre-pulse to +30 mV activated all channels to act as a reference for the later test pulse. Afterwards, the voltage was returned to the holding potential of -120 mV for 300 ms to allow recovery from inactivation. A 30 s inter-pulse to potentials in the range of -110 to 0 mV (in 10 mV steps) then drove the channels into slow inactivated states. Returning to the holding potential for 100 ms after that let channels in fast inactivated states recover from inactivation without inducing a significant recovery from slow inactivation. Finally, a test pulse to +30 mV activated all channels that did not undergo slow inactivation

during the inter-pulse. This pulse protocol was repeated every 90 seconds. The sodium current emerging at the test pulse (I_{test}) was then divided by the current at the pre-pulse (I_{pre}) and plotted against the voltage of the inter-pulse (V). The relationship between membrane voltage and the current ratio I_{test}/I_{pre} was again fitted with a Boltzmann function; G_{max} was set to 1.

After investigating steady-state slow inactivation we also recorded the time course of the onset of slow inactivation. The voltage protocol was mainly identical as described above for steady-state slow inactivation. This time, we did not vary the voltage of the inter-pulse but its duration. The voltage was always set to 0 mV and the duration varied between 72.9 s and 100 ms (decreased by factor 3 each time). We plotted the current ratio I_{test}/I_{pre} against the duration of the inter-pulse. The development of this ratio could be fitted with a two-phase exponential decay function similarly to the current decay described above.

Animals

$Na_v1.8$ knockout mice with C57BL/6 background, generated previously[24], were provided by Professor Stephen G. Waxman (Yale University School of Medicine, USA) and maintained in the animal center of Tongji Hospital, Wuhan. Genotyping was performed as described previously[24, 25]. The congenic wild-type mice were provided by the Animal Center of Hubei Province, China. All experimental protocols were performed with the approval of the ethical committee of Tongji Hospital, Tongji Medical College, Huazhong University of Science and Technology, and were performed in accordance with the National Institutes of Health guide for the care and use of Laboratory animals (NIH Publications No. 8023, revised 1978).

Repetitive behavioral tests

Spontaneous grooming test was performed as previously described[26]. Briefly, mice were individually placed in a transparent chamber without bedding for 10 minutes to habituate to the testing environment. After that, spontaneous grooming behavior was recorded for 10 minutes by video camera. Cumulative time spent in

spontaneous grooming all body regions was manually recorded and the behavior videotapes were evaluated in a blinded manner.

Nest building test

Nest building test was performed as previously described[27]. Briefly, the tested mice were transferred to individual cages overnight with food, water and new bedding. A 5 cm × 5 cm pressed cotton square was placed in each cage. The nests formed by the mice were assessed the next morning on a 5-point scale[27]. Nesting scores show the amount of cotton used.

Buried-food finding test

Buried-food finding test was performed as previously described[28]. Briefly, mice were deprived from food and water for one night before the test. On the day of the test, mice were individually placed in a clean cage with fresh bedding, where a food pellet was buried under 2 cm of bedding. The tested mouse was put into the cage and the latency to find the food pellet was recorded manually.

Three-chamber social test

Three-chamber social test was performed as previously described[29]. A social three-compartmented apparatus was used. The apparatus is divided in left, right and center chambers which includes two transparent sliding doors. The steps of the test were as followed:

1. Before sociability testing, the tested mouse (mouse No.1) was allowed to habituate to the testing environment. The tested mouse was placed in the central chamber with the sliding doors closed for 10 minutes.
2. Then, opening the sliding doors, the mouse No.1 was allowed to explore the sided chambers for 10 minutes which contained an empty cage respectively.
3. After habituation, an unfamiliar mouse (mouse No.2) with the same genetic background, age and sex was housed in the cage in one of the chambers, while the other chamber contains the same empty cage as mentioned in step 2. During the third 10 minutes session, the mouse No.1 was placed in the central chamber with the sliding doors opening. The tests were video-recorded, and time spent in each chamber was measured manually. The time spent in contact with the empty cage

(object) or with mouse No.2 in the cage were calculated.

4. During the fourth 10 minutes session, another unfamiliar mouse (mouse No.3) with same background, age and sex was housed in the empty cage in one of the side chambers. Mouse No.1 was placed in the central chamber and allowed to explore for 10 minutes with the sliding doors opening. The time spent in each chamber, contacting with the familiar mouse No.2 and unfamiliar mouse No.3 were assessed.

Statistical analysis

Patch-clamp data

Two-phase exponential decay fits were performed with Igor Pro Version 6.37 (WaveMetrics Inc., Portland, OR, USA). All other fits were performed with GraphPad Prism 5 (GraphPad Software, San Diego, CA, USA). Figures were created with CorelDRAW X6 (Corel Corporation, Ottawa, Canada). Unless otherwise specified, data are presented as mean ± 95% confidence interval (95% CI) and significance was assumed when $p < 0.05$. For all comparisons, data were first tested for normal distribution via D'Agostino-Pearson test. Whenever normally distributed, comparisons were done by Student's *t* test, otherwise the Mann-Whitney test was used. A sensitivity power analysis was performed to determine minimal detectable effects (MDE) using G*Power Version 3.1.9.7[30]. The following parameters were set to compute Cohen's *d* as MDE: $\alpha = 0.05$, $1 - \beta = 0.95$, and sample sizes *n* of the individual experiments. The minimal detectable difference (MDD) was calculated afterwards for each experiment. Results of the power analysis are summarized in *Supplementary Table 2*.

Animal data

The data of the animal experiment are expressed as mean ± standard error of the mean (SEM). Normal distribution test was performed before the analysis. Data of spontaneous grooming test and nest building test were analyzed by Student's two tailed, unpaired *t* test. Data of buried-food finding test were analyzed by

Mann-Whitney test. Data of three-chamber test were analyzed by two-way repeated ANOVA with a post-hoc paired-samples *t* test.

Results

Clinical picture

The patient is a six-year-old boy, and he was firstly admitted to the local hospital with intelligence and behavioral development problems when he was 2.5 years old. During the pregnancy, natural delivery and raising the child, there was no obvious abnormity according to his parents. In other family members, no similar cases can be found. Test of development quotient[31] was made, and the results showed that he had delayed development in adaptation, gross motor, communicational, cognitive and social-emotional skills. Magnetic resonance imaging was performed but no obvious abnormality was found. Tests regarding 48 types of congenital metabolic diseases including amino acid, organic acid and fatty acid metabolism were normal, as well as the chromosome karyotypic analysis. We asked the patient's mother to perform the Kirschner behavioral scale for autism (score: 14) and ABC behavioral[32] screening for autism (score: 47), both of which indicated the possibility of the patient being afflicted with ASD. When he was two years and 10 months old, the patient was diagnosed with ASD in a local psychiatric center, and he was included in rehabilitation training for children with autism.

When he was five years old, the patient was sent to another psychiatric center that confirmed the diagnosis. Chinese version of Psychoeducational Profile[33] was tested with a total score of 53, and delayed development in the skills of imitation, sensation, gross motor, fine motor, cognitive and language were identified. Recently, at the age of six the patient performed an intelligence quotient test using the Chinese version of the Wechsler Preschool and Primary Scale of Intelligence[34] and the total score was less than 45 (language intelligence quotient < 41, and operation intelligence quotient = 50), indicating mental retardation. In addition, as described by his parents, the patient shows decreased sensitivity to painful stimuli in comparison to other children. Quantitative sensory testing[35] was not performed due to the patients' health status.

Genetic screening and mutation analysis

The screening chip analysis showed that two heterozygous mutations in *SCN10A* (Chr3:38752440, 1534G>A and Chr3:38701963, 4533C>G; NC_000003.12) were identified, and Sanger sequencing was performed to validate the results (Figure 1A). No other specific mutation related to the patient was found in the whole genome sequencing and whole exome sequencing for the patient through high-throughput sequencing. The results of Sanger sequencing for the patient and his family members in three generations are shown in Figure 1B. Only the patient with two compound-heterozygous *SCN10A* mutations has been diagnosed with ASD, which conforms to laws of autosomal recessive inheritance.

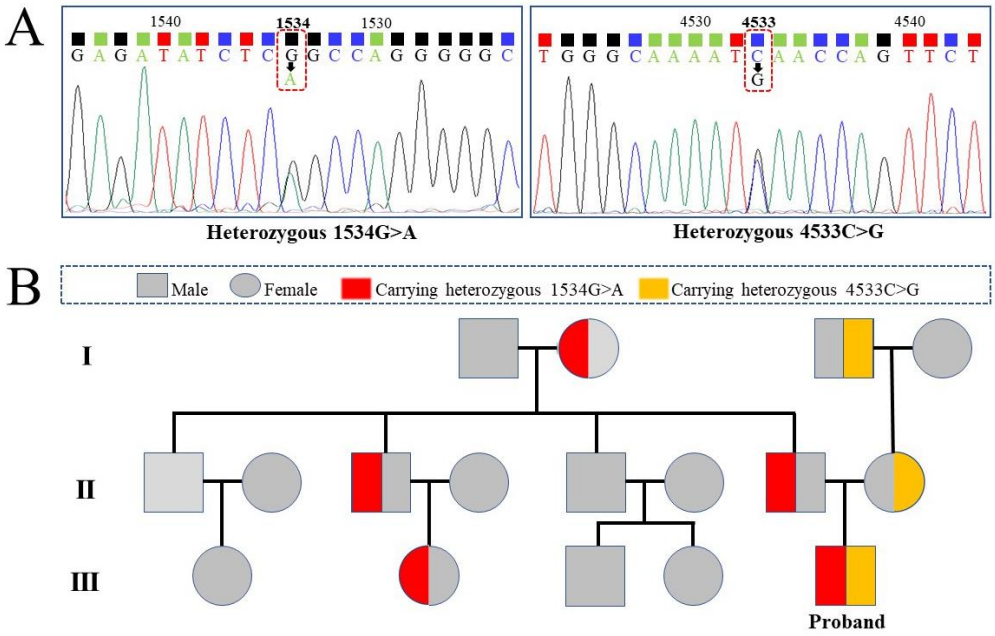

Figure 1. (A) Identified heterozygous *SCN10A* mutations in the patient. (B) Genetic linkage map for the patient and his family members in three generations.

The *SCN10A* mutation 1534G>A causes the amino acid arginine at 512th site to be substituted by the stop codon UGA, which would prematurely truncate the $Na_v1.8$ protein translation (Figure 2A,). The mutation 4533C>G would cause isoleucine at 1511th site to be substituted by methionine. Species conservative analysis showed that isoleucine was conserved across different species (Figure 2B). All function analysis

based on three different predicted tools (SIFT, prediction score -2.811; Ploy phen-2, prediction score 1.000; Mutation Taster, prediction score 0.960) conformably showed that p.I1511M can affect the protein function of $Na_v1.8$ (Figure 2C).

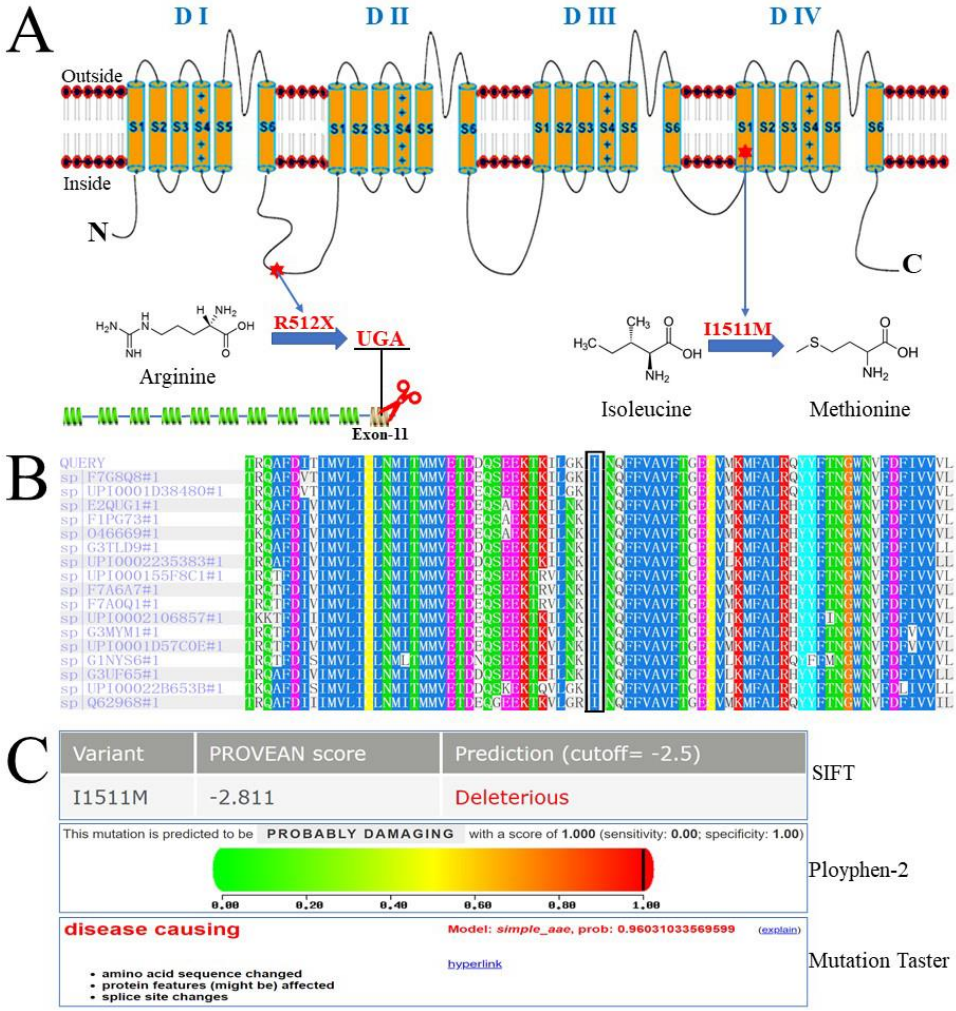

Figure 2. (A) The mutation sites for two heterozygous *SCN10A* mutations in $Na_v1.8$. (B) Species conservative analysis for I1511M. (C) Function prediction analysis for I1511M.

Truncation mutation $Na_v1.8$/R512X leads to loss-of-function

To test for the functional impact of the identified mutations we performed whole-cell voltage-clamp analysis. ND7/23 cells transfected with the WT $hNa_v1.8$ plasmid produced fast gating inward sodium current (n = 19, Figure 3A). However, cells transfected with $hNa_v1.8$ R512X failed to show significant sodium currents in all investigated cells (n = 9, Figure 3A, B). Thus, the truncation mutation p.R512X results in a functional knockout of the $hNa_v1.8$ channel.

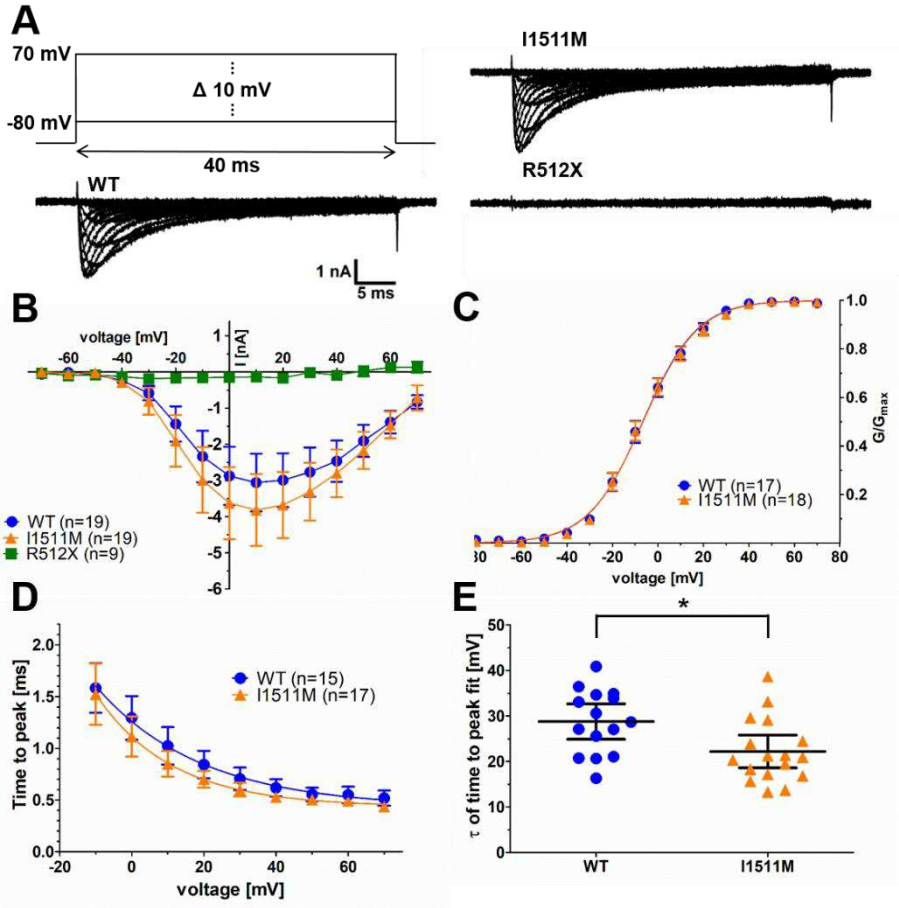

Figure 3. (A) Representative current traces for cells transfected with hNav1.8 WT (left trace), I1511M (upper right trace) or R512X (lower right trace). The voltage protocol is shown above the WT trace. (B) Current-voltage relationship of hNav1.8 WT, I1511M and R512X. (C) Conductance-voltage relationship of sodium channel activation of hNav1.8 WT and I1511M. (D) Development of time to peak values of hNav1.8 WT and I1511M over the different voltages. Both data sets were fitted with an exponential decay function. (E) Comparison of the values of the decay constant τ of the individual fits of the time to peak plots. *$p < 0.05$.

The $Na_v1.8$/I1511M mutation speeds up activation

In contrast to the p.R512X mutation, the p.I1511M mutation produced inward sodium current with comparable size to the WT channels (Fig. 3A, B). The mutated channels activated with the same voltage-dependence as WT (Fig. 3C, V_{half} of activation: -6.6 ± 2.1 mV, n = 17 [WT] vs. -6.6 ± 2.0 mV, n = 18 [I1511M], p = 0.95, slope factor k of the Boltzmann function: 11.8 ± 0.5, n = 17 [WT] vs. 11.85 ± 0.6, n =

18 [I1511M], $p = 0.80$).

The mean time to peak over a range of voltages of WT and I1511M channels were fitted with an exponential decay function (Fig. 3D), and revealed a faster τ for the I1511M mutation (Fig. 3E, 28.8 ± 3.9 mV, $n = 15$ [WT] vs. 22.2 ± 3.6 mV, $n = 17$ [I1511M], $p = 0.01$). Thus, the I1511M mutation shows a steeper voltage dependence in the development of time to peak values. Comparison of current density yielded no difference between WT and I1511M (Fig. 4A, -227.4 ± 52.7 pA/pF, $n = 25$ [WT] vs. -255.5 ± 61.6 pA/pF, $n = 25$ [I1511M], $p = 0.57$). Both the WT and the mutated channels produced robust persistent current up to 15% of the peak current (Fig. 4B), which did not differ between WT and Nav1.8/I1511M either (Fig. S2C, -30.9 ± 5.8 pA/pF, $n = 25$ [WT] vs. -37.9 ± 8.6 pA/pF, $n = 25$ [I1511M], $p = 0.17$).

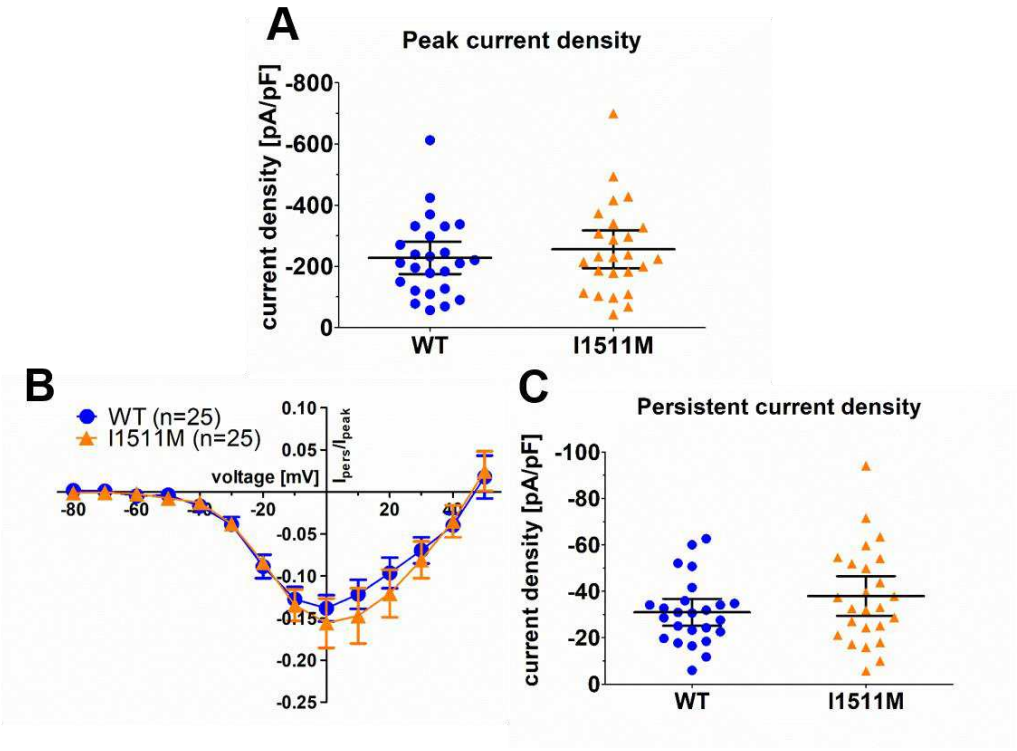

Figure 4. (A) Comparison of peak current density of the cells between hNav1.8 WT and I1511M. (B) Plot of current fraction remaining as persistent current (I_{pers}/I_{peak}) against the respective voltage. (C) Comparison of persistent current density of the cells between hNav1.8 WT and I1511M.

$Na_v1.8$/I1511M fast inactivation has faster kinetics than WT $Na_v1.8$

Voltage dependence of sodium channel fast inactivation of WT and I1511M channels was similar for both conditions (Fig. 5A, V_{half} : -71.2 ± 2.1 mV, n = 13 [WT] vs. -73.8 ± 2.3 mV, n = 15 [I1511M], p = 0.08, slope factor k: 10.5 ± 1.1, n = 13 [WT] vs. 10.6 ± 1.0, n = 15 [I1511M], p = 0.93). Nevertheless, current decay after activation, when fitted with a two-phase exponential decay (Fig. 5B), revealed a quicker τ_{fast}, suggesting speeding of entry of mutated Nav1.8 channels into fast inactivation (Fig. 5C, E). This is also reflected by a smaller area under the curve for the fast inactivation time constant (Fig. 5C, E, 15.6 ± 3.5 ms*mV, n = 13 [WT] vs. 12.0 ± 1.9 ms*mV, n = 16 [I1511M], $p < 0.05$) whereas τ_{slow} remained unaffected (Fig. 3D, F, 98.4 ± 13.1 ms*mV, n = 13 [WT] vs. 95.9 ± 11.7 ms*mV, n = 12 [I1511M], p = 0.76). These results represent an overall quicker current decay for the mutation.

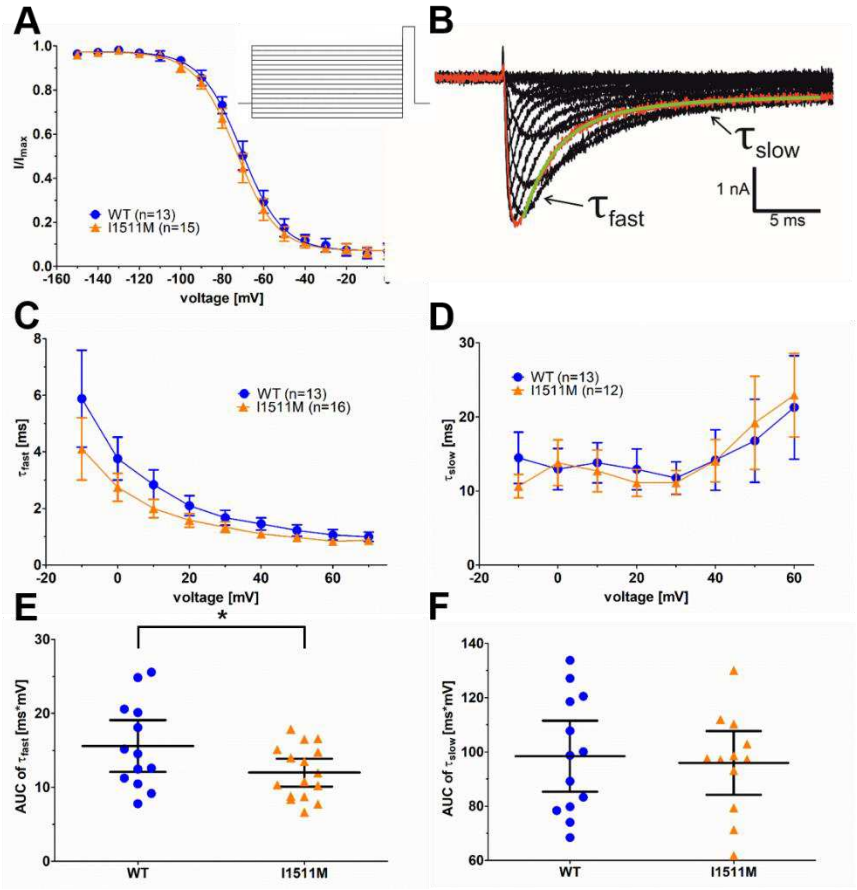

Figure 5. (A) Current-voltage relationship of sodium channel fast inactivation for $hNa_v1.8$ WT and I1511M. The voltage protocol is shown as inset. (B) Example trace for the current decay fit. The trace marked in red was fitted with a two-phase exponential decay function shown in green. The two components of the decay function with their respective decay

constant are indicated by arrows. (C) Development of τ_{fast} values over the different voltages. (D) Development of τ_{slow} values over the different voltages. (E) Comparison of the AUC of τ_{fast} plots for every cell. (F) Comparison of the AUC of τ_{slow} plots for every cell. *$p < 0.05$.

$Na_v1.8$/I1511M slow inactivation is enhanced

We investigated both the voltage dependence of steady-state slow inactivation and the time course of the onset of slow inactivation. Voltage-dependence of steady-state slow inactivation was unaffected by the mutation (Fig. 6A, -72.0 ± 4.4 mV, n = 15 [WT] vs. -73.6 ± 4.3 mV, n = 14 [I1511M], p = 0.74, slope factor k: 7.4 ± 0.7, n = 15 [WT] vs. 8.8 ± 1.5, n = 14 [I1511M], p = 0.21). Interestingly, the fraction of channels resisting slow inactivation at higher voltages was reduced (Fig. 6B, offset: 0.45 ± 0.05, n = 15 [WT] vs. 0.37 ± 0.05, n = 14 [I1511M], p = 0.03). Thus, at more depolarized voltages, a higher fraction of mutated channels enters the slow inactivated state and therefore fewer channels remain available.

Onset of slow inactivation was fitted with a two-phase exponential decay function, resulting in similar τ_{fast} and τ_{slow} (Fig. 6C, *Supplementary Table 3*). However, the AUC between WT and I1511M was reduced (Fig. 6D, 36.3 ± 3.4 ms*mV, n = 12 [WT] vs. 31.1 ± 2.7, n = 15 [I1511M], p = 0.02), which goes well in line with the smaller offset observed for steady-state slow inactivation at higher potentials. This difference indicates that over the different durations of the inter-pulse, the mutated channels are generally more likely to enter the slow inactivated state.

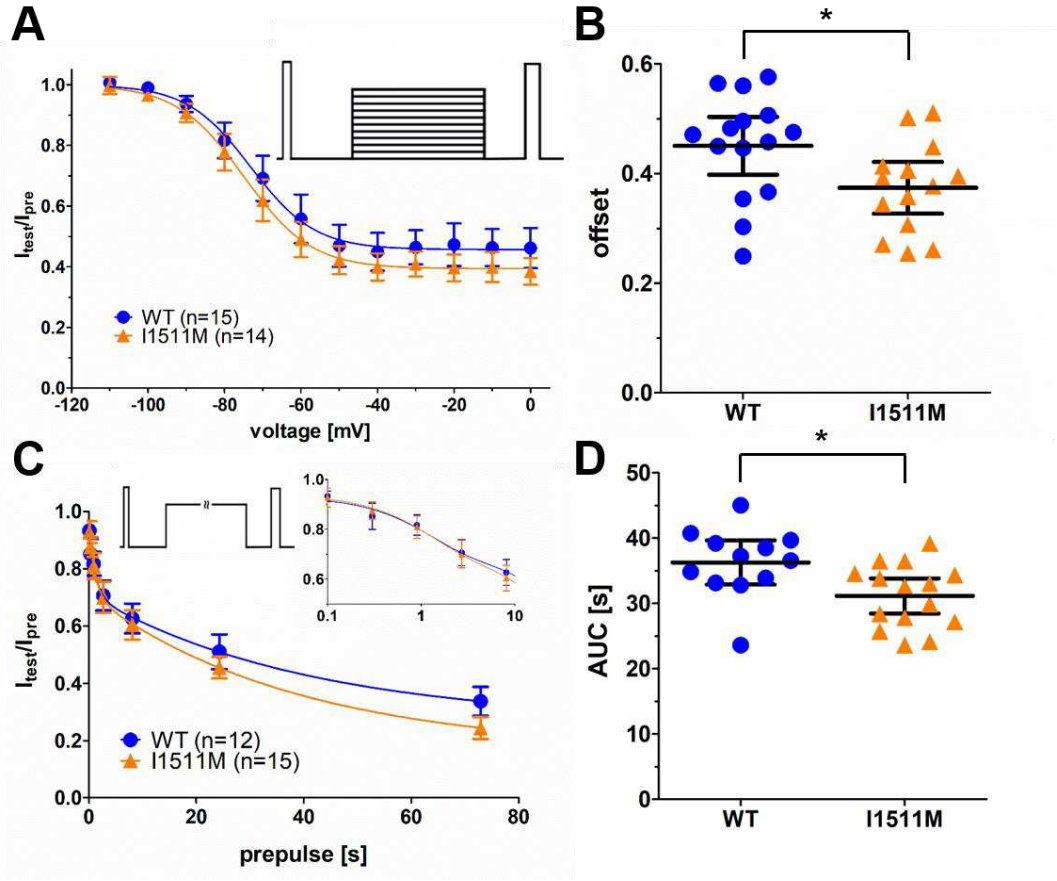

Figure 6. (A) Current-voltage relationship of sodium channel slow inactivation for hNa$_v$1.8 WT and I1511M. The voltage protocol is shown as inset. (B) Comparison of the offset of the Boltzmann fit of slow inactivation for each cell. (C) Development of current ratio I_{test}/I_{pre} over the different inter-pulse durations. Magnification of shorter inter-pulse durations on a logarithmic x-axis as well as the voltage protocol are shown as inset. (D) Comparison of the AUC of the onset of slow inactivation plots of each cell. *$p < 0.05$.

Autism-like behavior in Na$_v$1.8 knockout mice.

To explore the potential role of loss-of-function Na$_v$1.8 mutations in ASD, we tested for a potential autism-related phenotype of Na$_v$1.8 knockout mice by behavior experiments. Increased repetitive behavior is a common symptom in ASD patients. Repetitive behavior in rodents can be analyzed by a spontaneous grooming test[36]. In the self-grooming test, the time spent in self-grooming of Na$_v$1.8 knockout mice were higher than that of wild type mice (Fig. 7A). Nest building is one of the behaviors in mice, which has been reported to be associated with home-cage social

behaviors[37, 38]. $Na_v1.8$ knockout mice showed less nest building compared to wild type mice in this task. As shown in Figure 7B, the nesting scores in $Na_v1.8$ knockout mice were lower than that of wild type mice. The olfactory system is very important for social communication in rodents. Therefore, we examined the latency to find a buried food to rule out olfactory impairment of $Na_v1.8$ knockout mice before social interaction test. In buried-food finding test, the latency to find the food did not differ between wild type mice and $Na_v1.8$ knockout (Fig. 7C).

The three-chamber test is a reliable method for evaluating social behavior in rodents[39]. The tested mouse was allowed to freely explore and interact with object or mice placed in lateral chambers. The time in each chamber and the time in interaction with each stimulus were calculated. As shown in Figure 7D-E, wild type mice spent more time in the chamber with another mouse than in the chamber with an object, suggesting intact social behavior. In contrast, $Na_v1.8$ knockout mice showed lack of preference for either the object or the other mouse. Compared with wild type mice, $Na_v1.8$ knockout mice showed decreased interaction with the social stimulus (in this case, the second mouse). In the next step, the object was replaced by a novel, unfamiliar mouse, while the familiar mouse remained accessible as well. Wild type mice showed preferential interaction with the novel mouse than with the familiar mouse. In contrast, $Na_v1.8$ knockout mice spent increased time in the chamber with the familiar mouse and decreased time in the chamber with the novel mouse. In addition, $Na_v1.8$ knockout mice spent similar time interacting with the familiar and the novel mouse (Fig. 7G). Compared with wild type mice, $Na_v1.8$ knockout mice displayed reduced interaction with a novel mouse (Fig. 7F-G). These results showed impaired social behavior of $Na_v1.8$ knockout mice.

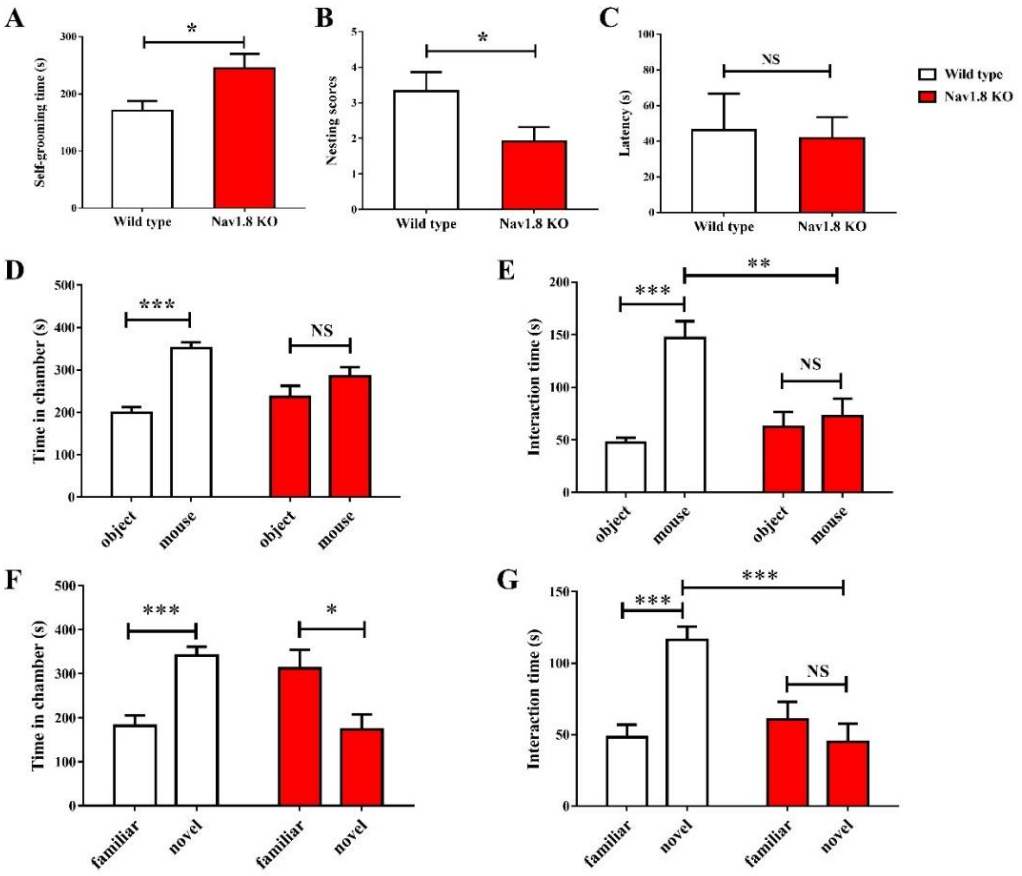

Figure 7. ASD-related behavioral tests in $Na_v1.8$ knockout mice. (A) Self-grooming test. Increased self-grooming time in $Na_v1.8$ knockout mice. (B) Nest building test. $Na_v1.8$ knockout mice had a poor score in nest building. (C) Buried-food finding test. There were no differences in the latency to find a buried food pellet between wild type mice and $Na_V1.8$ knock-out mice. (D-G) Three-chamber social test. $Na_v1.8$ knockout mice showed a lack of preference for social (mouse) and non-social (object) stimuli and a lack of preference for novel stimuli. n = 12 (A-B) and n = 9 (C-G) mice per group. *p < 0.05, **p < 0.01, ***p < 0.001.

Discussion

In the present study, we identified a patient with ASD, which is possibly caused by two novel compound-heterozygous *SCN10A* mutations. Through electrophysiological examination, we found that both mutations lead to different degrees of loss-of-function in $Na_v1.8$. In addition, behavioral experiments showed that $Na_v1.8$ knockout mice present behavioral abnormalities that are in line with a typical ASD phenotype.

The most apparent symptoms of ASD comprise deficits in social interaction or repetitive, stereotypical behavior. Accordingly, these symptoms can be found in the diagnostic criteria of this group of neurodevelopmental disorders[40]. But additionally, a significant fraction of ASD patients also show abnormal reactions to environmental stimuli such as somatosensory input[41]. In fact, hyper- or hyporeactivity to different stimuli can act as predictor for diagnosis and/or severity of ASD[42, 43]. The social impairment that is most prominent in many ASD cases may also be the result of this altered perception of the environment. It has been shown that sensory abnormalities in early life relate to the development of social symptoms in children diagnosed with ASD[44].

The molecular mechanisms underlying these somatosensory abnormalities are associated with distinct peripheral somatosensory neurons, such as low-threshold mechanoreceptors (LTMRs) which are responsible for the perception of innocuous tactile stimuli[45, 46]. Apart from the mainly studied myelinated Aβ- and Aδ-LTMRs, there are also unmyelinated LTMRs (C-LTMRs, reviewed in [47]), that are suggested to play a role both in neuropathic pain[48] and affective or social touch[49], showing another connection between sensory perception and social interaction.

There is also growing evidence for an involvement of nociceptive neurons in ASD pathophysiology, as ASD patients often show abnormal reactions to potentially painful stimuli[50-52]. This involvement of nociceptors is well in line with the observations in our patient, which was reported to be less sensitive to painful stimuli. This fits our hypothesis of a role of $Na_v1.8$ in the pathogenesis of ASD in the patient, because $Na_v1.8$ is expressed in nociceptors and is important for their function.

Another link between ASD and $Na_v1.8$ can be found in the example of *SHANK3*, which is a scaffolding protein that has been found to be responsible for a subset of monogenetic ASD cases[53, 54]. Mutations in *SHANK3* are also linked to another neurodevelopmental disorder, the Phelan-McDermid syndrome[55]. This syndrome also shows prominent changes in somatosensory responses, namely hyperreactivity to light touch and at the same time hyporeactivity to painful stimuli[56, 57]. On a molecular basis, apart from different brain regions, *SHANK3* can be found at

presynaptic terminals of somatosensory neurons in the dorsal horn of the spinal cord[58, 59]. Han *et al.*[58] observed a marked reduction of nociceptive behavior in mice with *SHANK3* haploinsufficiency. They found reduced pain responses in models of inflammatory as well as neuropathic pain especially concerning heat hyperalgesia. This effect could be narrowed down to interaction of *SHANK3* with *TRPV1* in neurons positive for $Na_v1.8$.

VGSCs such as $Na_v1.8$ are responsible for the fast upstroke of the action potential and are thus an important regulator of neuronal excitability. Neuronal excitability is commonly implicated in pathophysiological theories of ASD. Especially the theory of excitatory/inhibitory imbalance[9] offers a way of explaining ASD symptoms. Alterations of VGSCs could create such an imbalance and therefore cause autistic traits. Accordingly, VGSC isoforms expressed preferentially in the brain, such as $Na_v1.1$ and $Na_v1.2$[60-62], but also $Na_v1.7$[63], which can be found in nociceptors, were already linked to ASD. $Na_v1.8$, which is preferentially expressed in the peripheral nervous system, has so far not been associated with ASD. $Na_v1.8$ was shown to be involved in diseases of the peripheral nervous system, such as chronic pain disorders[64-67], and arrhythmias[68]. The channel's expression pattern and its associated diseases suggest a mainly peripheral effect $Na_v1.8$ and its mutations. Our investigated mutations represent a loss-of-function of the channel. Interestingly, loss-of-function in the isoform $Na_v1.7$, which is also mainly expressed in the peripheral nervous system, cause the disorder congenital insensitivity to pain (CIP)[69]. This disease does not show any signs of autistic symptoms in affected patients. Therefore, one could hypothesize that loss of function in $Na_v1.8$ may affect peripheral neurons in a different way than loss of function in $Na_v1.7$.

Another explanation would be an additional involvement of $Na_v1.8$ also in the central nervous system. In fact, the channel can be found in the CNS[70], offering the possibility of a broader involvement in neurological diseases. Additionally, recent research from Kambouris et al. revealed mutations in *SCN10A* that can be linked to epilepsy[10].

The cardinal symptoms of our patient include mental retardation, reduced verbal

skills and hyperactivity. Through next-generation sequencing including 6110 possibly related genes, we found two heterozygous *SCN10A* mutations (one missense mutation and one terminator mutation). Both of the two mutations were not reported before. We verified the screening results and investigated his parents using Sanger sequencing, which indicated that it is in accordance with the separation of Mendelian law. Both parents carry one of the mutations, and do not show signs of ASD. Thus, the genetic data indicated that the combined occurrence of the screened *SCN10A* mutation may account for the patient's symptoms. However, *SCN10A* was mostly correlated to pain phenotypes before, questioning the mutations to be responsible for ASD. Thus, we further carried out whole genome sequencing and a whole exome sequencing, but failed to detect another potential mutation site except for the *SCN10A* mutations.

To investigate possible functional changes introduced by the two mutations, electrophysiological experiments were performed. The results of our examinations reveal that the p.R512X mutation leads to a complete functional knockout of the channel. Therefore, all $Na_v1.8$ function in the patient's neurons arises from channels carrying the p.I1511M mutation. Our detailed patch-clamp experiment regarding this mutation show a slight loss-of-function regarding a speeded entry of fast inactivation as well as an enhanced slow inactivation. We conclude that these changes in the channel's biophysical properties may lead to impaired function of $Na_v1.8$-expressing neurons and to an altered neuronal development. This alteration may have led to the deficits that the patient developed and which resulted in the diagnosis of ASD. Adding to our *in vitro* data from patch-clamp experiments, we investigated $Na_v1.8$ knockout mice to check for ASD-like behavior. And in fact, we saw several changes in behavior compared to wild type mice that demonstrate autistic traits in the knockout mice.

Limitations

However, there are some limitations in this study. First, we only verified the functions of p.I1511M and p.R512X mutations *in vitro*. The functions of these mutations *in vivo* need to be further verified. The mice with these mutations can be

constructed to verify the mutation functions in the future investigations. Second, since we have only found one ASD patient which may relate to *SCN10A* mutations, the role of $Na_v1.8$ in ASD needs to be confirmed in more cases. Third, the cellular mechanism underlying the effect of Nav1.8 on ASD needed to be explored in future studies.

Conclusion

In summary, this study expands the potential function of *SCN10A* in autism according to the evidence at molecular, *in vivo* and human level. Our work presents $Na_v1.8$ as a protein potentially involved in ASD pathophysiology and adds to the knowledge about the genetic basis of the disorder.

Abbreviations

ASD: Autism spectrum disorder

DMEM: Dulbecco's modified Eagle's medium

ECS: extracellular solution

MDD: minimal detectable difference

MDE: minimal detectable effects

SEM: standard error of the mean

TTP: time to peak

VGSC: voltage-gated sodium channel

WT: wild type

Declarations

Ethics approval and consent to participate

The study regarding this rare case of ASD was approved by the hospital ethics

committee of The Second Affiliated Hospital of Chongqing Medical University, and informed consent was obtained from all subjects.

All experimental protocols were performed with the approval of the ethical committee of Tongji Hospital, Tongji Medical College, Huazhong University of Science and Technology, and were performed in accordance with the National Institutes of Health guide for the care and use of Laboratory animals (NIH Publications No. 8023, revised 1978).

Consent for publication

Not applicable.

Availability of data and materials

All data can be acquired from corresponding author through email.

Competing interests

The authors declare no conflict of interest.

Funding

This work was supported by National Natural Science Foundation of China (NO.81701096), by the Deutsche Forschungsgemeinschaft (DFG, German Research Foundation, LA2740/3-1; 363055819/GRK2415 to A.L. 368482240/GRK2416 to A.L. and M.R. RO4046/2-1 and /2-2, Emmy Noether Program to M.R.) and by a grant from the Interdisciplinary Centre for Clinical Research within the faculty of Medicine at the RWTH Aachen University (IZKF TN1-8/IA 532008, TN1-7 532007).). B.N. is supported by a grant from the Interdisciplinary Center for Clinical Research within the faculty of Medicine at the RWTH Aachen University.

Author' Contributions

All authors approved the final manuscript.

Björn Heinrichs designed, performed, analyzed and interpreted patch clamp experiments and wrote the manuscript.

Baowen Liu performed behavioral experiments, and wrote the manuscript.

Jin Zhang performed behavioral experiments.

Jannis E. Meents designed, analyzed and interpreted patch clamp experiments.

Kim Le interpreted the data and revised the manuscript.

Petra Hautvast performed mutagenesis experiments.

Xiwen Zhu performed patch clamp experiments.

Ningbo Li analyzed and interpreted the patient data.

Yi Liu analyzed and interpreted the patient data.

Markus Rothermel interpreted the data and revised the manuscript.

Barbara Namer interpreted the data and revised the manuscript.

Xianwei Zhang conceived the study, analyzed, interpreted and discussed the data.

Angelika Lampert conceived the study, analyzed, interpreted and discussed the data, participated in writing and revised the manuscript.

Guangyou Duan conceived the study, interpreted and discussed the data, participated in writing and revised the manuscript.

Acknowledgments

We would like to thank the patient and his family members' selfless contribution to this work. We thank Professor Stephen G. Waxman for kindly providing $Na_v1.8$ knockout mice. We thank Brigitte Hoch for excellent technical assistance.

References

1. Baron-Cohen S, Scott FJ, Allison C, Williams J, Bolton P, Matthews FE, Brayne C: **Prevalence of autism-spectrum conditions: UK school-based population study**. *Br J Psychiatry* 2009, **194**(6):500-509.

2. Christensen DL, Baio J, Van Naarden Braun K, Bilder D, Charles J, Constantino JN, Daniels J, Durkin MS, Fitzgerald RT, Kurzius-Spencer M *et al*: **Prevalence and Characteristics of Autism Spectrum Disorder Among Children Aged 8 Years--Autism**

and Developmental Disabilities Monitoring Network, 11 Sites, United States, 2012. *MMWR Surveill Summ* 2016, **65**(3):1-23.

3. Xu G, Strathearn L, Liu B, O'Brien M, Kopelman TG, Zhu J, Snetselaar LG, Bao W: **Prevalence and Treatment Patterns of Autism Spectrum Disorder in the United States, 2016**. *JAMA Pediatr* 2019, **173**(2):153-159.

4. Sandin S, Lichtenstein P, Kuja-Halkola R, Larsson H, Hultman CM, Reichenberg A: **The familial risk of autism**. *JAMA* 2014, **311**(17):1770-1777.

5. Tick B, Colvert E, McEwen F, Stewart C, Woodhouse E, Gillan N, Hallett V, Lietz S, Garnett T, Simonoff E *et al*: **Autism Spectrum Disorders and Other Mental Health Problems: Exploring Etiological Overlaps and Phenotypic Causal Associations**. *J Am Acad Child Adolesc Psychiatry* 2016, **55**(2):106-113 e104.

6. Colvert E, Tick B, McEwen F, Stewart C, Curran SR, Woodhouse E, Gillan N, Hallett V, Lietz S, Garnett T *et al*: **Heritability of Autism Spectrum Disorder in a UK Population-Based Twin Sample**. *JAMA Psychiatry* 2015, **72**(5):415-423.

7. Amaral DG: **Examining the Causes of Autism**. *Cerebrum* 2017, **2017**.

8. Yoon SH, Choi J, Lee WJ, Do JT: **Genetic and Epigenetic Etiology Underlying Autism Spectrum Disorder**. *J Clin Med* 2020, **9**(4).

9. Rubenstein JL, Merzenich MM: **Model of autism: increased ratio of excitation/inhibition in key neural systems**. *Genes Brain Behav* 2003, **2**(5):255-267.

10. Kambouris M, Thevenon J, Soldatos A, Cox A, Stephen J, Ben-Omran T, Al-Sarraj Y, Boulos H, Bone W, Mullikin JC *et al*: **Biallelic SCN10A mutations in neuromuscular disease and epileptic encephalopathy**. *Ann Clin Transl Neurol* 2017, **4**(1):26-35.

11. Harkin LA, McMahon JM, Iona X, Dibbens L, Pelekanos JT, Zuberi SM, Sadleir LG, Andermann E, Gill D, Farrell K *et al*: **The spectrum of SCN1A-related infantile epileptic encephalopathies**. *Brain* 2007, **130**(Pt 3):843-852.

12. Lampert A, O'Reilly AO, Reeh P, Leffler A: **Sodium channelopathies and pain**. *Pflugers Arch* 2010, **460**(2):249-263.

13. Renganathan M, Cummins TR, Waxman SG: **Contribution of Na(v)1.8 sodium channels to action potential electrogenesis in DRG neurons**. *J Neurophysiol* 2001, **86**(2):629-640.

14. Liu XD, Yang JJ, Fang D, Cai J, Wan Y, Xing GG: **Functional upregulation of nav1.8 sodium channels on the membrane of dorsal root Ganglia neurons contributes to the development of cancer-induced bone pain**. *PLoS One* 2014, **9**(12):e114623.

15. O'Brien MS, Philpott HTA, McDougall JJ: **Targeting the Nav1.8 ion channel engenders sex-specific responses in lysophosphatidic acid-induced joint neuropathy**. *Pain* 2019, **160**(1):269-278.

16. Li N, Liu B, Wu W, Hong Y, Zhang J, Liu Y, Zhang M, Zhang X, Duan G: **Upregulation of transcription factor 4 downregulates NaV1.8 expression in DRG neurons and prevents the development of rat inflammatory and neuropathic hypersensitivity**. *Exp Neurol* 2020, **327**:113240.

17. Riquelme I, Hatem SM, Montoya P: **Abnormal Pressure Pain, Touch Sensitivity, Proprioception, and Manual Dexterity in Children with Autism Spectrum Disorders**. *Neural Plast* 2016, **2016**:1723401.

18. Failla MD, Moana-Filho EJ, Essick GK, Baranek GT, Rogers BP, Cascio CJ: **Initially**

intact neural responses to pain in autism are diminished during sustained pain. *Autism* 2018, **22**(6):669-683.

19. Tordjman S, Anderson GM, Charrier A, Oriol C, Kermarrec S, Canitano R, Botbol M, Coulon N, Antoine C, Brailly-Tabard S *et al*: **Relationships Between Self-Injurious Behaviors, Pain Reactivity, and beta-Endorphin in Children and Adolescents With Autism**. *J Clin Psychiatry* 2018, **79**(2).

20. de la Torre-Ubieta L, Won H, Stein JL, Geschwind DH: **Advancing the understanding of autism disease mechanisms through genetics**. *Nat Med* 2016, **22**(4):345-361.

21. Vaser R, Adusumalli S, Leng SN, Sikic M, Ng PC: **SIFT missense predictions for genomes**. *Nat Protoc* 2016, **11**(1):1-9.

22. Adzhubei I, Jordan DM, Sunyaev SR: **Predicting functional effect of human missense mutations using PolyPhen-2**. *Curr Protoc Hum Genet* 2013, **Chapter 7**:Unit7 20.

23. Schwarz JM, Cooper DN, Schuelke M, Seelow D: **MutationTaster2: mutation prediction for the deep-sequencing age**. *Nat Methods* 2014, **11**(4):361-362.

24. Nassar MA, Stirling LC, Forlani G, Baker MD, Matthews EA, Dickenson AH, Wood JN: **Nociceptor-specific gene deletion reveals a major role for Nav1.7 (PN1) in acute and inflammatory pain**. *Proc Natl Acad Sci U S A* 2004, **101**(34):12706-12711.

25. Gautron L, Sakata I, Udit S, Zigman JM, Wood JN, Elmquist JK: **Genetic tracing of Nav1.8-expressing vagal afferents in the mouse**. *J Comp Neurol* 2011, **519**(15):3085-3101.

26. Zike ID, Chohan MO, Kopelman JM, Krasnow EN, Flicker D, Nautiyal KM, Bubser M, Kellendonk C, Jones CK, Stanwood G *et al*: **OCD candidate gene SLC1A1/EAAT3**

impacts basal ganglia-mediated activity and stereotypic behavior. *Proc Natl Acad Sci U S A* 2017, **114**(22):5719-5724.

27. Deacon RM: **Assessing nest building in mice**. *Nat Protoc* 2006, **1**(3):1117-1119.

28. Yang M, Crawley JN: **Simple behavioral assessment of mouse olfaction**. *Curr Protoc Neurosci* 2009, **Chapter 8**:Unit 8 24.

29. Schmeisser MJ, Ey E, Wegener S, Bockmann J, Stempel AV, Kuebler A, Janssen AL, Udvardi PT, Shiban E, Spilker C *et al*: **Autistic-like behaviours and hyperactivity in mice lacking ProSAP1/Shank2**. *Nature* 2012, **486**(7402):256-260.

30. Faul F, Erdfelder E, Lang AG, Buchner A: **G*Power 3: a flexible statistical power analysis program for the social, behavioral, and biomedical sciences**. *Behav Res Methods* 2007, **39**(2):175-191.

31. Kawabe K, Kondo S, Matsumoto M, Seo K, Ochi M, Oka Y, Horiuchi F, Ueno SI: **Developmental quotient to estimate intelligence in autism spectrum disorder**. *Pediatr Int* 2016, **58**(10):963-966.

32. Fung LK, Mahajan R, Nozzolillo A, Bernal P, Krasner A, Jo B, Coury D, Whitaker A, Veenstra-Vanderweele J, Hardan AY: **Pharmacologic Treatment of Severe Irritability and Problem Behaviors in Autism: A Systematic Review and Meta-analysis**. *Pediatrics* 2016, **137 Suppl 2**:S124-135.

33. Wang M, Jiang L, Tang X: **Levetiracetam is associated with decrease in subclinical epileptiform discharges and improved cognitive functions in pediatric patients with autism spectrum disorder**. *Neuropsychiatr Dis Treat* 2017, **13**:2321-2326.

34. Huang C, Martorell R, Ren A, Li Z: **Cognition and behavioural development in early**

childhood: the role of birth weight and postnatal growth. *Int J Epidemiol* 2013, **42**(1):160-171.

35. Rolke R, Baron R, Maier C, Tolle TR, Treede RD, Beyer A, Binder A, Birbaumer N, Birklein F, Botefur IC *et al*: **Quantitative sensory testing in the German Research Network on Neuropathic Pain (DFNS): standardized protocol and reference values**. *Pain* 2006, **123**(3):231-243.

36. Rabaneda LG, Robles-Lanuza E, Nieto-Gonzalez JL, Scholl FG: **Neurexin dysfunction in adult neurons results in autistic-like behavior in mice**. *Cell Rep* 2014, **8**(2):338-346.

37. Penagarikano O, Abrahams BS, Herman EI, Winden KD, Gdalyahu A, Dong H, Sonnenblick LI, Gruver R, Almajano J, Bragin A *et al*: **Absence of CNTNAP2 leads to epilepsy, neuronal migration abnormalities, and core autism-related deficits**. *Cell* 2011, **147**(1):235-246.

38. Szczypka MS, Kwok K, Brot MD, Marck BT, Matsumoto AM, Donahue BA, Palmiter RD: **Dopamine production in the caudate putamen restores feeding in dopamine-deficient mice**. *Neuron* 2001, **30**(3):819-828.

39. Yang M, Silverman JL, Crawley JN: **Automated three-chambered social approach task for mice**. *Curr Protoc Neurosci* 2011, **Chapter 8**:Unit 8 26.

40. American Psychiatric Association: **Autism Spectrum Disorder**. In: *Diagnostic and Statistical Manual of Mental Disorders.* 5th edn. Washington, DC; 2013.

41. Tomchek SD, Dunn W: **Sensory processing in children with and without autism: a comparative study using the short sensory profile**. *Am J Occup Ther* 2007, **61**(2):190-200.

42. Grzadzinski R, Donovan K, Truong K, Nowell S, Lee H, Sideris J, Turner-Brown L, Baranek GT, Watson LR: **Sensory Reactivity at 1 and 2 Years Old is Associated with ASD Severity During the Preschool Years**. *J Autism Dev Disord* 2020.

43. Jussila K, Junttila M, Kielinen M, Ebeling H, Joskitt L, Moilanen I, Mattila ML: **Sensory Abnormality and Quantitative Autism Traits in Children With and Without Autism Spectrum Disorder in an Epidemiological Population**. *J Autism Dev Disord* 2020, **50**(1):180-188.

44. Baranek GT, Woynaroski TG, Nowell S, Turner-Brown L, DuBay M, Crais ER, Watson LR: **Cascading effects of attention disengagement and sensory seeking on social symptoms in a community sample of infants at-risk for a future diagnosis of autism spectrum disorder**. *Dev Cogn Neurosci* 2018, **29**:30-40.

45. Orefice LL: **Peripheral Somatosensory Neuron Dysfunction: Emerging Roles in Autism Spectrum Disorders**. *Neuroscience* 2020.

46. Orefice LL, Zimmerman AL, Chirila AM, Sleboda SJ, Head JP, Ginty DD: **Peripheral Mechanosensory Neuron Dysfunction Underlies Tactile and Behavioral Deficits in Mouse Models of ASDs**. *Cell* 2016, **166**(2):299-313.

47. Liljencrantz J, Olausson H: **Tactile C fibers and their contributions to pleasant sensations and to tactile allodynia**. *Front Behav Neurosci* 2014, **8**:37.

48. Liljencrantz J, Bjornsdotter M, Morrison I, Bergstrand S, Ceko M, Seminowicz DA, Cole J, Bushnell MC, Olausson H: **Altered C-tactile processing in human dynamic tactile allodynia**. *Pain* 2013, **154**(2):227-234.

49. Loken LS, Wessberg J, Morrison I, McGlone F, Olausson H: **Coding of pleasant touch**

by unmyelinated afferents in humans. *Nat Neurosci* 2009, **12**(5):547-548.

50. Tordjman S, Anderson GM, Botbol M, Brailly-Tabard S, Perez-Diaz F, Graignic R, Carlier M, Schmit G, Rolland AC, Bonnot O *et al*: **Pain reactivity and plasma beta-endorphin in children and adolescents with autistic disorder**. *PLoS One* 2009, **4**(8):e5289.

51. Klintwall L, Holm A, Eriksson M, Carlsson LH, Olsson MB, Hedvall A, Gillberg C, Fernell E: **Sensory abnormalities in autism. A brief report**. *Res Dev Disabil* 2011, **32**(2):795-800.

52. Moore DJ: **Acute pain experience in individuals with autism spectrum disorders: a review**. *Autism* 2015, **19**(4):387-399.

53. Sheng M, Kim E: **The Shank family of scaffold proteins**. *J Cell Sci* 2000, **113 (Pt 11)**:1851-1856.

54. Moessner R, Marshall CR, Sutcliffe JS, Skaug J, Pinto D, Vincent J, Zwaigenbaum L, Fernandez B, Roberts W, Szatmari P *et al*: **Contribution of SHANK3 mutations to autism spectrum disorder**. *Am J Hum Genet* 2007, **81**(6):1289-1297.

55. Phelan K, McDermid HE: **The 22q13.3 Deletion Syndrome (Phelan-McDermid Syndrome)**. *Mol Syndromol* 2012, **2**(3-5):186-201.

56. Philippe A, Boddaert N, Vaivre-Douret L, Robel L, Danon-Boileau L, Malan V, de Blois MC, Heron D, Colleaux L, Golse B *et al*: **Neurobehavioral profile and brain imaging study of the 22q13.3 deletion syndrome in childhood**. *Pediatrics* 2008, **122**(2):e376-382.

57. Sarasua SM, Boccuto L, Sharp JL, Dwivedi A, Chen CF, Rollins JD, Rogers RC,

Phelan K, DuPont BR: **Clinical and genomic evaluation of 201 patients with Phelan-McDermid syndrome**. *Hum Genet* 2014, **133**(7):847-859.

58. Han Q, Kim YH, Wang X, Liu D, Zhang ZJ, Bey AL, Lay M, Chang W, Berta T, Zhang Y *et al*: **SHANK3 Deficiency Impairs Heat Hyperalgesia and TRPV1 Signaling in Primary Sensory Neurons**. *Neuron* 2016, **92**(6):1279-1293.

59. Orefice LL, Mosko JR, Morency DT, Wells MF, Tasnim A, Mozeika SM, Ye M, Chirila AM, Emanuel AJ, Rankin G *et al*: **Targeting Peripheral Somatosensory Neurons to Improve Tactile-Related Phenotypes in ASD Models**. *Cell* 2019, **178**(4):867-886 e824.

60. Weiss LA, Escayg A, Kearney JA, Trudeau M, MacDonald BT, Mori M, Reichert J, Buxbaum JD, Meisler MH: **Sodium channels SCN1A, SCN2A and SCN3A in familial autism**. *Mol Psychiatry* 2003, **8**(2):186-194.

61. O'Roak BJ, Deriziotis P, Lee C, Vives L, Schwartz JJ, Girirajan S, Karakoc E, Mackenzie AP, Ng SB, Baker C *et al*: **Exome sequencing in sporadic autism spectrum disorders identifies severe de novo mutations**. *Nat Genet* 2011, **43**(6):585-589.

62. Sanders SJ, Murtha MT, Gupta AR, Murdoch JD, Raubeson MJ, Willsey AJ, Ercan-Sencicek AG, DiLullo NM, Parikshak NN, Stein JL *et al*: **De novo mutations revealed by whole-exome sequencing are strongly associated with autism**. *Nature* 2012, **485**(7397):237-241.

63. Rubinstein M, Patowary A, Stanaway IB, McCord E, Nesbitt RR, Archer M, Scheuer T, Nickerson D, Raskind WH, Wijsman EM *et al*: **Association of rare missense variants in the second intracellular loop of NaV1.7 sodium channels with familial autism**. *Mol Psychiatry* 2018, **23**(2):231-239.

64. Faber CG, Lauria G, Merkies IS, Cheng X, Han C, Ahn HS, Persson AK, Hoeijmakers JG, Gerrits MM, Pierro T *et al*: **Gain-of-function Nav1.8 mutations in painful neuropathy**. *Proc Natl Acad Sci U S A* 2012, **109**(47):19444-19449.

65. Huang J, Yang Y, Zhao P, Gerrits MM, Hoeijmakers JG, Bekelaar K, Merkies IS, Faber CG, Dib-Hajj SD, Waxman SG: **Small-fiber neuropathy Nav1.8 mutation shifts activation to hyperpolarized potentials and increases excitability of dorsal root ganglion neurons**. *J Neurosci* 2013, **33**(35):14087-14097.

66. Han C, Vasylyev D, Macala LJ, Gerrits MM, Hoeijmakers JG, Bekelaar KJ, Dib-Hajj SD, Faber CG, Merkies IS, Waxman SG: **The G1662S NaV1.8 mutation in small fibre neuropathy: impaired inactivation underlying DRG neuron hyperexcitability**. *J Neurol Neurosurg Psychiatry* 2014, **85**(5):499-505.

67. Kist AM, Sagafos D, Rush AM, Neacsu C, Eberhardt E, Schmidt R, Lunden LK, Orstavik K, Kaluza L, Meents J *et al*: **SCN10A Mutation in a Patient with Erythromelalgia Enhances C-Fiber Activity Dependent Slowing**. *PLoS One* 2016, **11**(9):e0161789.

68. Bezzina CR, Barc J, Mizusawa Y, Remme CA, Gourraud JB, Simonet F, Verkerk AO, Schwartz PJ, Crotti L, Dagradi F *et al*: **Common variants at SCN5A-SCN10A and HEY2 are associated with Brugada syndrome, a rare disease with high risk of sudden cardiac death**. *Nat Genet* 2013, **45**(9):1044-1049.

69. Cox JJ, Reimann F, Nicholas AK, Thornton G, Roberts E, Springell K, Karbani G, Jafri H, Mannan J, Raashid Y *et al*: **An SCN9A channelopathy causes congenital inability to experience pain**. *Nature* 2006, **444**(7121):894-898.

70. Shields SD, Ahn HS, Yang Y, Han C, Seal RP, Wood JN, Waxman SG, Dib-Hajj SD: **Nav1.8 expression is not restricted to nociceptors in mouse peripheral nervous system**. *Pain* 2012, **153**(10):2017-2030.

Figures

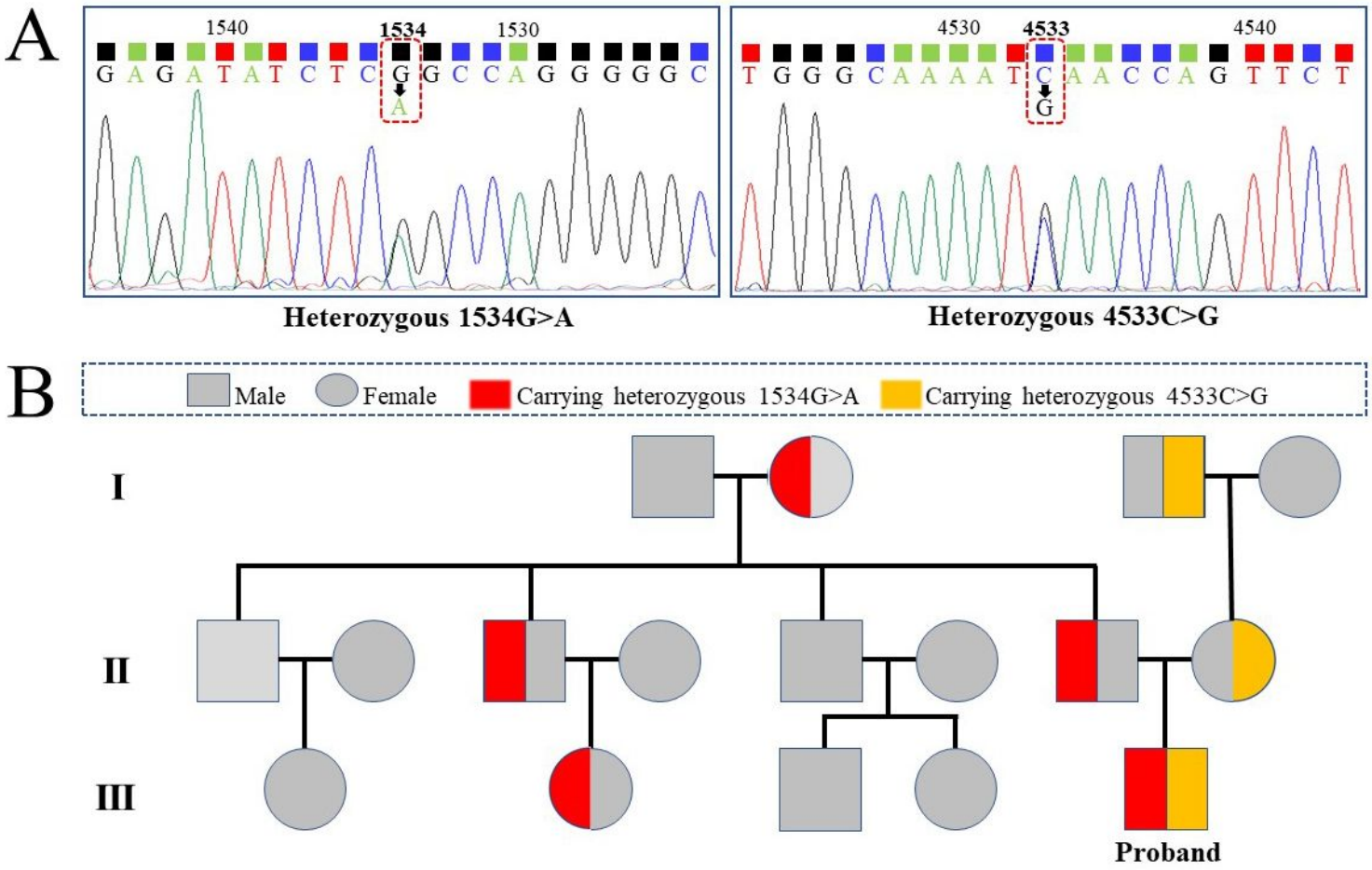

Figure 1

(A) Identified heterozygous SCN10A mutations in the patient. (B) Genetic linkage map for the patient and his family members in three generations.

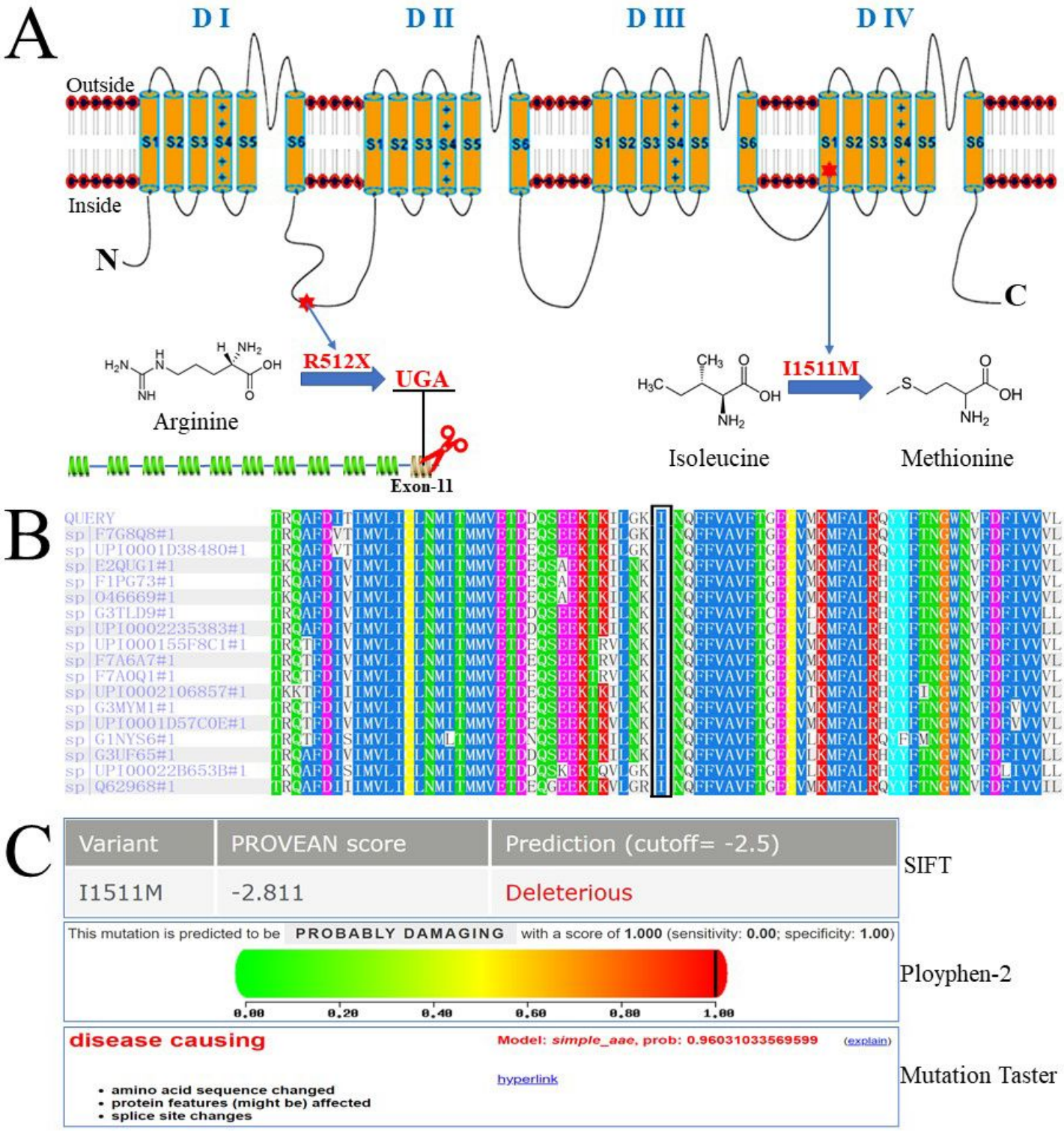

Figure 2

(A) The mutation sites for two heterozygous SCN10A mutations in Nav1.8. (B) Species conservative analysis for I1511M. (C) Function prediction analysis for I1511M.

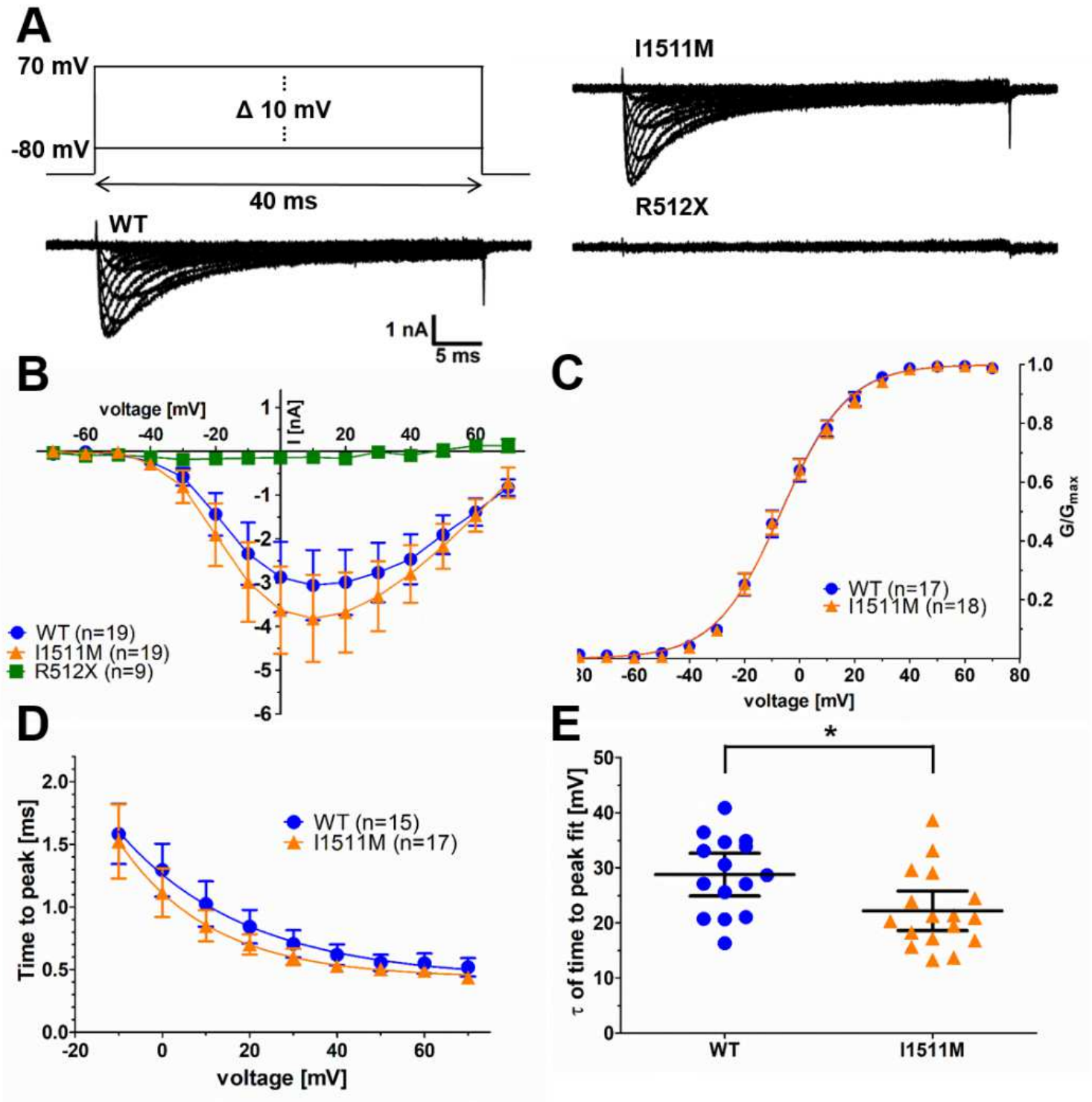

Figure 3

(A) Representative current traces for cells transfected with hNav1.8 WT (left trace), I1511M (upper right trace) or R512X (lower right trace). The voltage protocol is shown above the WT trace. (B) Current-voltage relationship of hNav1.8 WT, I1511M and R512X. (C) Conductance-voltage relationship of sodium channel activation of hNav1.8 WT and I1511M. (D) Development of time to peak values of hNav1.8 WT and I1511M over the different voltages. Both data sets were fitted with an exponential decay function. (E)

Comparison of the values of the decay constant τ of the individual fits of the time to peak plots. *p < 0.05.

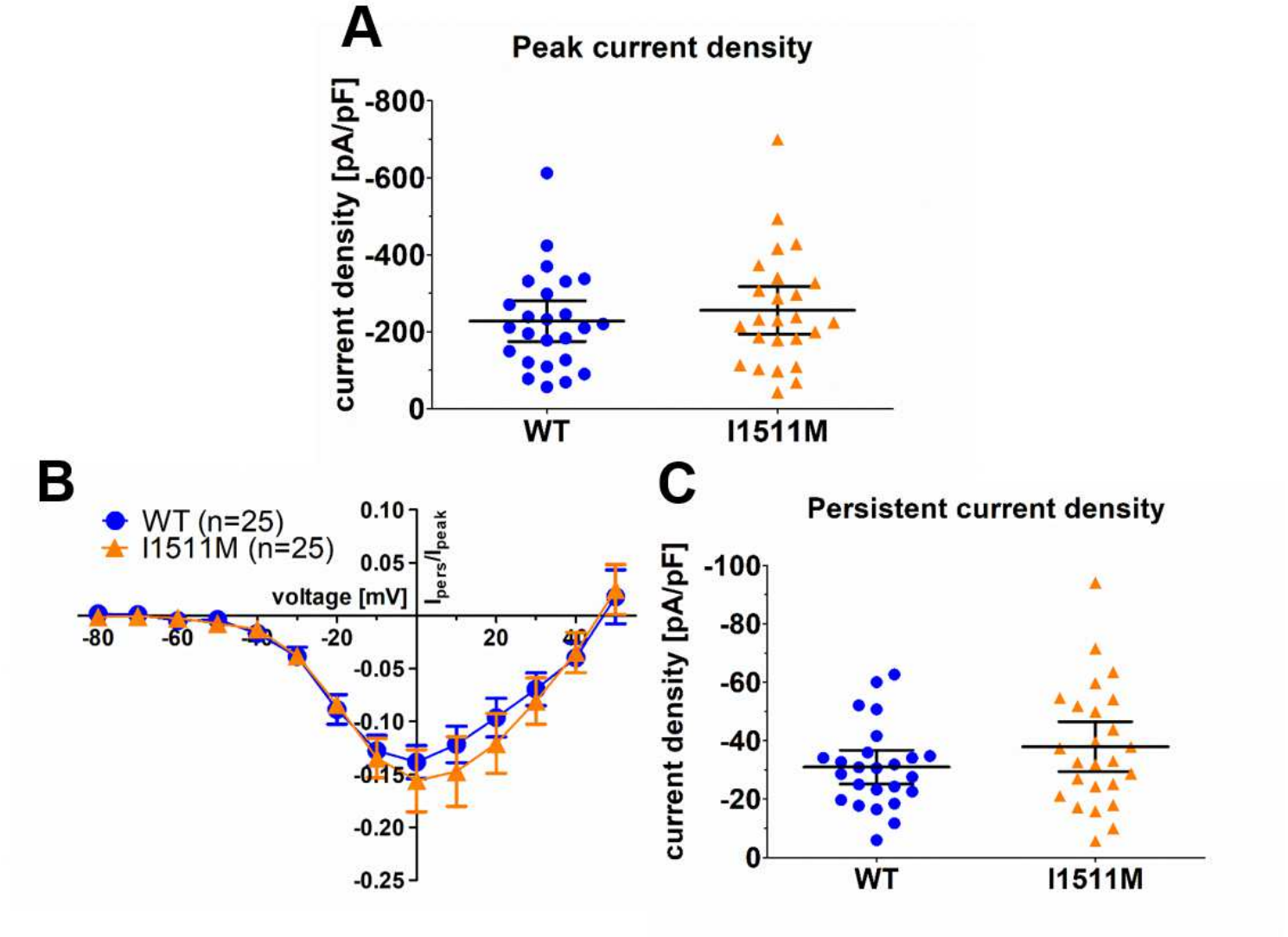

Figure 4

(A) Comparison of peak current density of the cells between hNav1.8 WT and I1511M. (B) Plot of current fraction remaining as persistent current (Ipers/Ipeak) against the respective voltage. (C) Comparison of persistent current density of the cells between hNav1.8 WT and I1511M.

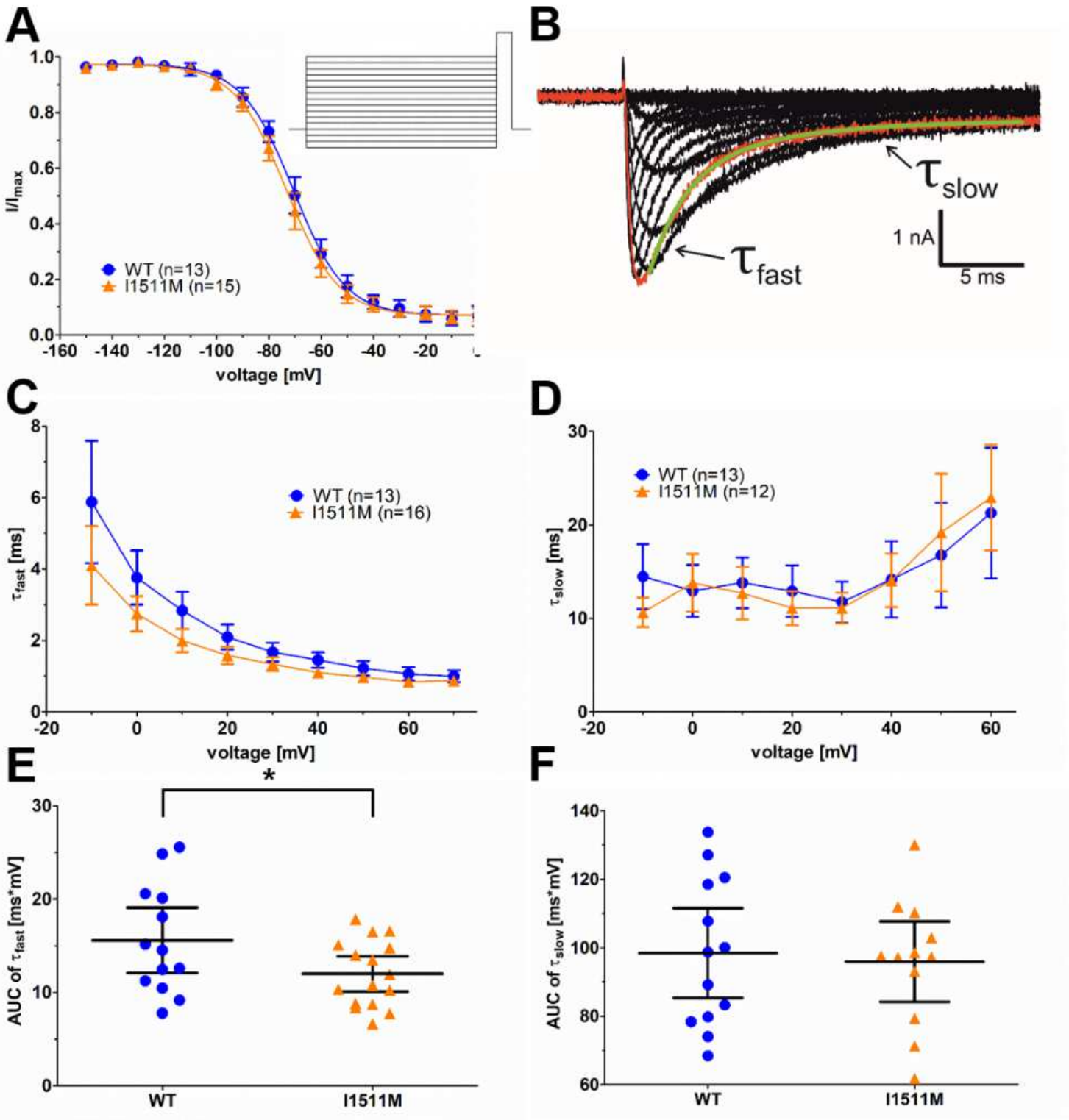

Figure 5

(A) Current-voltage relationship of sodium channel fast inactivation for hNav1.8 WT and I1511M. The voltage protocol is shown as inset. (B) Example trace for the current decay fit. The trace marked in red was fitted with a two-phase exponential decay function shown in green. The two components of the decay function with their respective decay constant are indicated by arrows. (C) Development of τfast values over the different voltages. (D) Development of τslow values over the different voltages. (E)

Comparison of the AUC of τfast plots for every cell. (F) Comparison of the AUC of τslow plots for every cell. *p < 0.05.

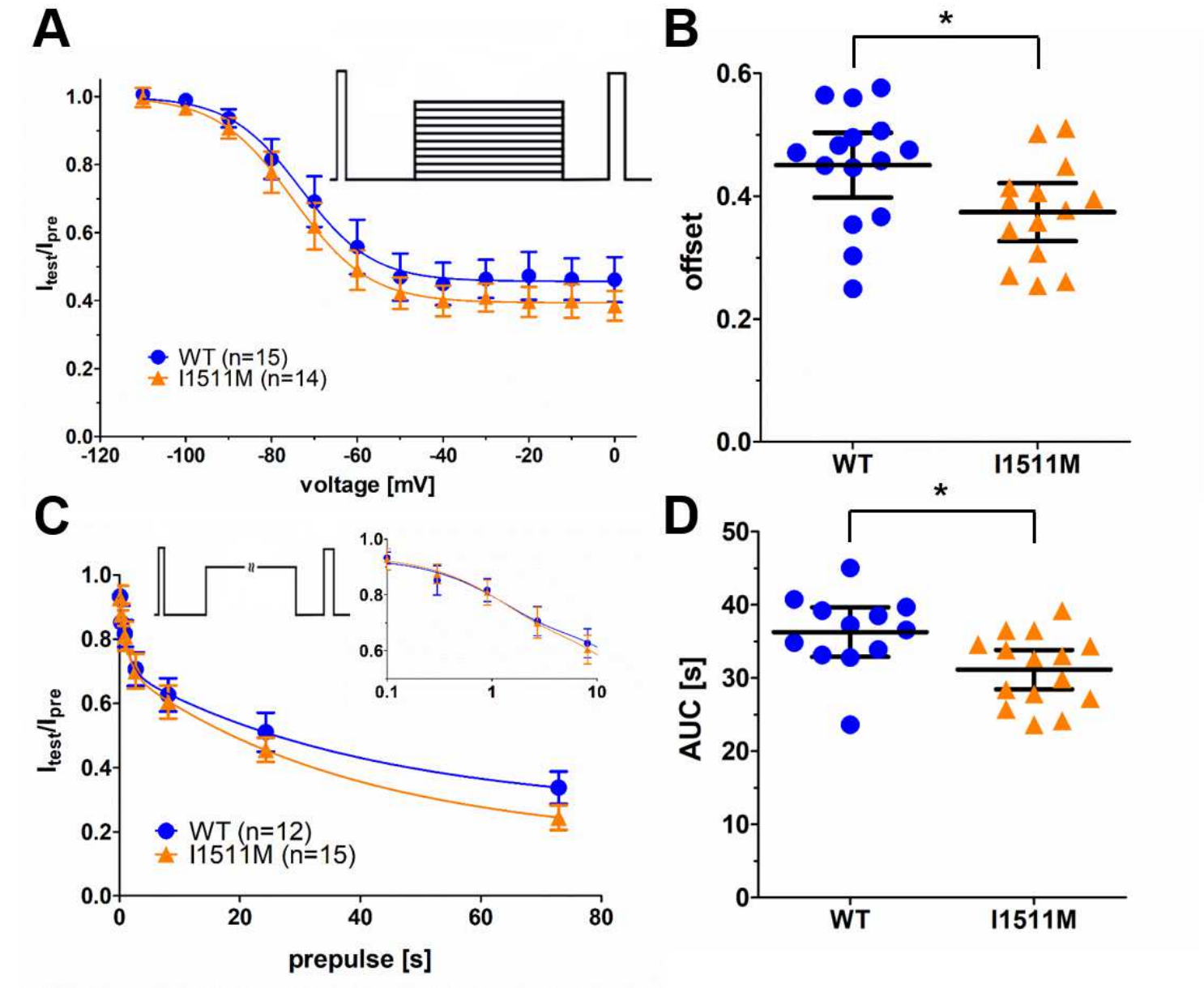

Figure 6

(A) Current-voltage relationship of sodium channel slow inactivation for hNav1.8 WT and I1511M. The voltage protocol is shown as inset. (B) Comparison of the offset of the Boltzmann fit of slow inactivation for each cell. (C) Development of current ratio Itest/Ipre over the different inter-pulse durations. Magnification of shorter inter-pulse durations on a logarithmic x-axis as well as the voltage protocol are shown as inset. (D) Comparison of the AUC of the onset of slow inactivation plots of each cell. *p < 0.05.

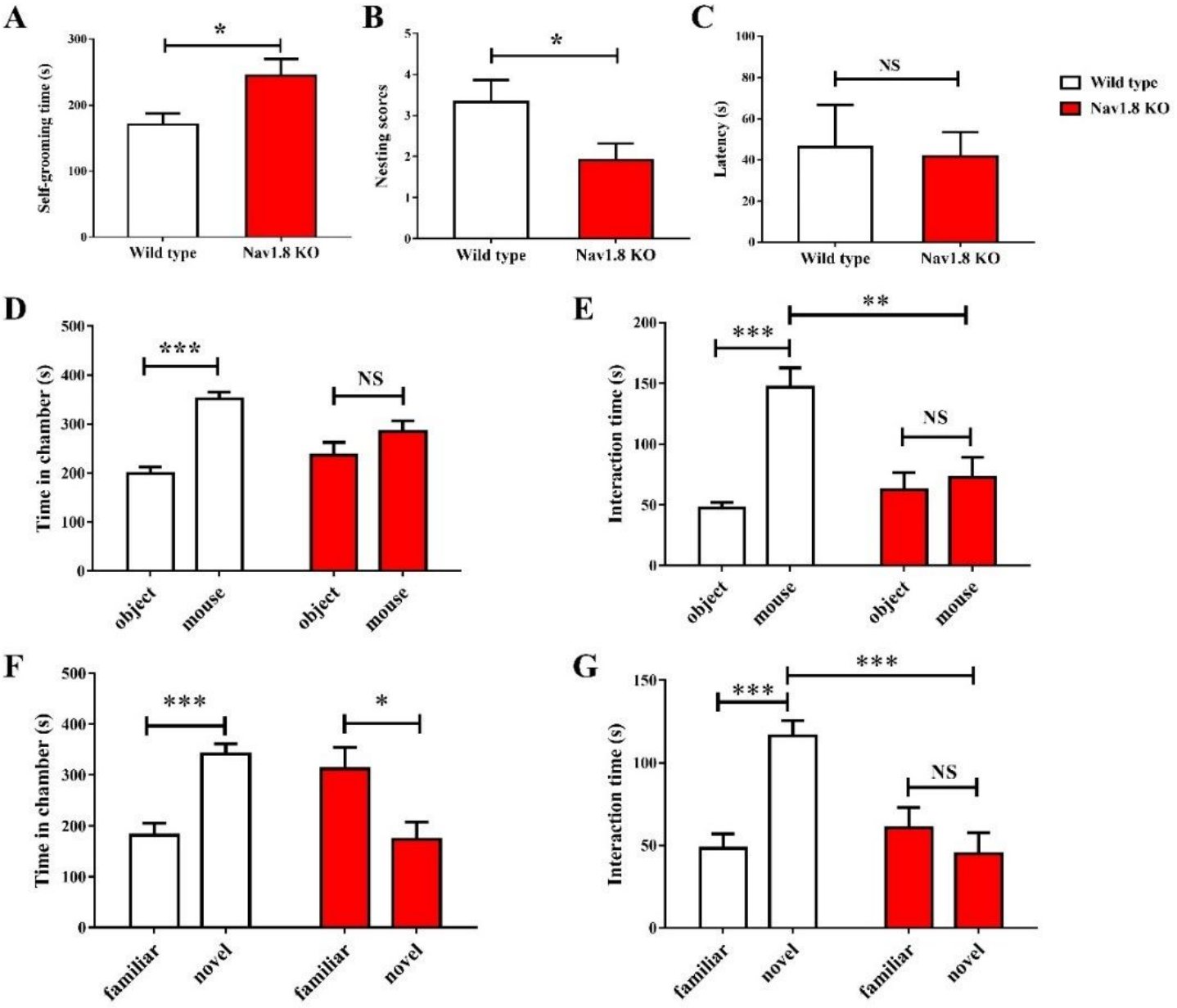

Figure 7

ASD-related behavioral tests in Nav1.8 knockout mice. (A) Self-grooming test. Increased self-grooming time in Nav1.8 knockout mice. (B) Nest building test. Nav1.8 knockout mice had a poor score in nest building. (C) Buried-food finding test. There were no differences in the latency to find a buried food pellet between wild type mice and NaV1.8 knock-out mice. (D-G) Three-chamber social test. Nav1.8 knockout mice showed a lack of preference for social (mouse) and non-social (object) stimuli and a lack of preference for novel stimuli. n = 12 (A-B) and n = 9 (C-G) mice per group. *p < 0.05, **p < 0.01, ***p < 0.001.

Supplementary Files

This is a list of supplementary files associated with this preprint. Click to download.

- Supplementarytable1.docx
- Supplementarytable3.docx
- Supplementarytable2.docx